Plasma Sources
Science and
Technology

Foundations of plasma-assisted combustion. Part 1: Fundamentals of combustion and plasma.

To cite this article before publication: Svetlana M Starikovskaia *et al* 2026 *Plasma Sources Sci. Technol.* in press https://doi.org/10.1088/1361-6595/ae3a17

Foundations of plasma-assisted combustion. Part 1: Fundamentals of combustion and plasma.

S M Starikovskaia[1], V Lafaurie[1], J-B Perrin-Terrin[2], C O Laux[2]

[1] Laboratoire de Physique des Plasmas (LPP), CNRS, Observatoire de Paris, Sorbonne Université, Université Paris-Saclay, École polytechnique, Institut Polytechnique de Paris, 91120 Palaiseau, France
[2] Université Paris-Saclay, CNRS, CentraleSupélec, Laboratoire EM2C, 91190 Gif-sur-Yvette, France

svetlana.starikovskaia@lpp.polytechnique.fr, christophe.laux@centralesupelec.fr

Abstract

The use of plasma as an innovative solution to enhance combustion has been the focus of intense research for the past two decades. Plasma-Assisted Ignition and Combustion (PAI/PAC) has emerged as a potential solution for numerous industrial applications. This Foundation paper consists of two parts. Part 1 introduces the context and is followed by a brief summary of the reviews done over the last two decades to show the continued relevance of the topic. We then focus on the fundamentals of combustion and introduce the main concepts of the field. In particular, we discuss combustion kinetics, flame propagation modes, and numerical modeling. Following this, a more in-depth description of plasma physics, specifically non-equilibrium plasma, is provided. As in the previous section, the main concepts are highlighted and defined. We discuss electron energy distribution functions, electron-impact cross-sections, and reaction rates, with a focus on dissociation and fast gas heating which are of particular relevance in the field of plasma-assisted combustion. Finally, elements of numerical modeling are provided. Part 2 of the article will describe the topic of plasma-assisted combustion from the description of fundamental mechanisms to novel combustion systems of importance for the energy transition.

Contents

1 Introduction: plasma-assisted combustion

The challenges associated with climate change are bringing a strong impetus to change the current energy production methods, which today are based for more than 80% on the combustion of fossil resources. The combustion of fossil fuels not only produces most anthropogenic CO_2 emissions [1] [2] but also generates pollutants, such as nitrogen oxides (NO_x), sulfur oxides (SO_x), unburned hydrocarbons (HC), particulates, and soot. These pollutants impact air quality and contribute both directly and indirectly to global warming mechanisms and acid rain. Ambitious recommendations have been set to reduce CO_2 and pollutant emissions in all sectors including transportation, energy turbines, industrial plants, and heating. As an example, Europe has recommended drastic measures for aviation with the 2050 goal to reduce CO_2 emissions by 75% and NO_x emissions by 90% relative to 2010 levels [1].

Although electrification will help alleviate CO_2 emissions, it is unlikely to entirely replace combustion for aircraft engines and other forms of long-haul transport, such as maritime transport [3], heating, or industrial furnaces. New strategies are currently being pursued to enable CO_2–free combustion with hydrogen or ammonia, or CO_2–neutral combustion with biofuels or sustainably produced hydrocarbons. However the combustion of these new fuels faces similar challenges as traditional fuels regarding the control of instabilities and the reduction of pollutants.

The use of plasma as an innovative solution to enhance combustion has been the focus of intense research for the past two decades. Plasma-Assisted Ignition and Combustion (PAI/PAC) has emerged as a potential solution to extend the ignition limits, to shift the lean blow-off limit, and to control combustion instabilities, thus helping reach the full potential of these novel systems. In a set of recent invited roadmaps [4–6], PAC topics were identified among about 20 key themes of modern plasma physics, further confirming growing interest for them in the community. Several review papers are available in the field.

The first review, published in 2006 by Starikovskaia [7], presents a summary of theoretical/experimental studies of nonequilibrium plasma applications for combustion. The main highlighted themes are ignition and combustion enhancement, as

well as comparisons of the efficiencies of thermal and nonequilibrium plasmas for ignition.

The same year, a special issue of IEEE Transactions on Plasma Science edited by Matveev and Rosocha [8] collected 10 papers discussing nonequilibrium plasma applications to combustion, particularly for enhancing combustion stability, efficiency, and reducing undesirable emissions.

A review by Adamovich *et al.* [9], published in 2009, analyzes non-thermal and thermal effects in plasma-assisted ignition and high-speed flow control. The review focuses on ignition enhancement by nanosecond repetitive dielectric barrier discharges (DBD) at low pressure.

The Handbook of Combustion, published in 2010, contains two chapters devoted to the interactions between low-temperature plasma and combustion. The first chapter by Starikovskaia *et al.* [10] gives a brief review of experimental data and theoretical approaches and the second chapter by Vincent-Randonnier [11] reviews available diagnostic tools to measure combustion enhancement and flame stabilization by plasma.

A series of review papers in 2011 and 2013 by Starikovskii *et al.* [12, 13] present experimental results obtained in different conditions, from supersonic flows to quiescent gases. A detailed analysis of the action of plasma on combustible mixtures is given. The authors discuss the evolution of the electron energy distribution function, or EEDF, and the associated energy branching in plasma. The hierarchy of energy relaxation is traced with examples taken from the literature. These reviews cover various aspects of plasma action on flames, distinguishing natural chemi-ionization within the flame from plasma-induced effects such as flow turbulization and the generation of radicals ahead of the flame front.

A 2014 topical review by Starikovskaia [14] considers ignition and combustion triggered or sustained by pulsed nanosecond discharges in different geometries. The benefits of pulsed high-voltage discharges for kinetic studies and for applications are demonstrated. The necessity and the possibilities to build a particular kinetic mechanism of plasma–assisted ignition and combustion are discussed. A map of pressure and temperature parameters ($P - T$ diagram) is proposed to unify the available data on ignition delay times, ignition lengths and densities of intermediate species reported in the literature.

A special issue of Philosophical Transactions of the Royal Society dedicated to the physics and chemistry of plasma-assisted combustion, edited by Starikovskii [15], was published in 2015. The issue contains 13 original papers on fast combustion waves, nitric oxides formation, ozone additions, and kinetic mechanisms.

A 2015 review by Ju *et al.* [16] discusses advances in understanding non-thermal

and thermal effects, kinetic pathways of atomic oxygen production, diagnostics of electronically and vibrationally excited species, plasma-combustion kinetics of sub-explosion limit ignition, plasma-assisted low temperature combustion, transitions of the classical ignition S-curve, and dynamics of the minimum ignition energy.

A 2016 topical review by Leonov *et al.* [17] presents an overview of experimental and modeling studies of near-surface discharges and their interaction with the air flow. Nonequilibrium energy partition and unsteady temporal behaviour significantly affect the flow even at a moderate Specific Energy Input (SEI). This is critical not only for plasma flow-control applications but also for plasma-assisted combustion in high-speed flows.

A 2017 review by Alrashidi *et al.* [18] classifies the ideas of plasma-assisted combustion in terms of applications to different types of engines. The authors provide summary tables with extensive information about different discharges, their parameters, method of diagnostics and approaches. They also discuss the efficiency of nonequilibrium plasmas for different types of engines.

A 2021 review by Starikovskaia *et al.* [19] describes theoretical problems related to kinetic modeling of plasma-assisted combustion, discusses the role of excited electronic states in enhancing reaction rates, and presents high pressure experiments for plasma-assisted combustion and experiments on plasma-assisted detonation.

A 2022 review by Laux [20] discusses flame stabilization and ignition by nanosecond repetitively pulsed discharges. The same year, a review by Popov *et al* [21] describes fast gas heating (FGH), which is the abrupt increase of gas temperature in nonequilibrium low-temperature plasmas due to relaxation of electronically excited states of atoms/molecules and charged species. Although the review mainly considers non-combustible gases and mixtures, a few experimental and theoretical studies of the fast gas heating in hydrogen- and hydrocarbon-containing mixtures are discussed and it is shown that the results in chemically inert mixtures can be transferred to combustible mixtures.

In 2023, a book chapter by Ju *et al.* [22] discusses progress in understanding the mechanisms and applications of plasma-assisted hydrogen combustion. The chemistry and dynamics of plasma-assisted hydrogen combustion are analyzed, and its applications in advanced engines are presented. The same year, a paper by Lacoste [23] reviews progress in plasma-assisted combustion with a special focus on flame dynamics including coupling between flames and acoustic waves.

The 2025 book of Ju and Starikovskii on Plasma Assisted Combustion and Chemical Processing [24] provides an introduction to the opportunities of plasma-assisted combustion and chemical processing for green energy conversion using renewable electricity. Covering the fundamentals of combustion and plasma physics and chem-

istry, it details the mechanisms and technologies of plasma-enhanced combustion, chemical processing, materials manufacturing and recycling, and pollutant control.

The authors hope the above, albeit brief, descriptions of reviews will be helpful to specialists and newcomers alike in the field to guide their selection of reading in the field of plasma-assisted combustion. The work undertaken in this tutorial review aims not to replace but to feed the wealth of reviews available in the field, with perhaps a stronger emphasis on the fundamentals so that plasma and combustion physicists may have an easier time understanding one-another. The review is written as a two-part article. The present article, corresponding to Part 1, is structured as follows. Section 2 introduces the fundamentals of combustion and combustion chemistry. Section 3 provides a more in-depth definition of the concept of "low-temperature nonequilibrium plasma", as well as an explanation of the role of electrons in chemical transformations occurring in such plasmas, in particular in the dissociation of molecules by electron impact. Part 2 of the article [25] describes the fundamental mechanisms and the applications of plasma-assisted combustion, both in laboratory experiments and in large-scale facilities.

2 Combustion

Combustion, one of humanity's earliest discoveries, has shaped technological progress and civilization for the past two centuries. Antoine-Laurent Lavoisier's law of mass conservation in 1772 [26], Dmitri Mendeleev's periodic table of chemical elements in 1869, and the kinetic theory of gases developed by James Clerk Maxwell and Ludwig Boltzmann in the latter half of the 19th century preceded the widespread use of combustion. In the 20th century, internal combustion engines (Benz, Diesel) and gas turbines revolutionized industry [27]. The chain theory of combustion later earned Semenov and Hinshelwood the Nobel Prize in 1956 [28–32].

2.1 Combustion: fundamental concepts

In his Nobel lecture, N.N. Semenov provided the following definition: "combustion or explosion process is a chemical reaction between the components of the combustible mixture, accompanied by the liberation of heat and various kinds of motion in gases". The discovery of branched chain reactions and the creation of a theory of these reactions marked the beginning of a new, important stage in the development of combustion science [33]. A principal discovery was that the high rates of chain combustion processes are determined by the reactions of highly active intermediate species: free atoms and radicals. We will return to this idea in a later discussion on plasma-assisted combustion because active species are key in plasma physics and

chemistry, and for now, turn to the definition of the fundamental concepts of combustion.

2.1.1 General considerations

Combustion is more than just chemistry; it is a complex physico-chemical process characterized by the exponentially rapid release of energy and the transition of a combustible mixture from one thermodynamic state to another. Describing this process requires a comprehensive understanding of hydrodynamics, thermodynamics, heat and mass transfer, and chemical kinetics. Covering the entire theory of combustion is not possible within this topical review. We will concentrate on basic terms and definitions, and refer the reader seeking more detailed information to classic combustion theory books for those seeking more detailed information [34–38].

Combustion needs fuel and oxidizer. In the present review, oxygen or air will be considered as the oxidizer. The combustion regime is defined by three important features: the phase of the reactants, the degree of fuel-oxidizer mixing, and the flow dynamic regime. In this article, we will specifically focus on gas-phase combustion without discussing liquid and solid fuels. In this sense, we will always consider *homogeneous* combustion (distinct from *heterogeneous* combustion where the reactants initially exist in different phases). When fuel and oxidizer are injected separately in the combustion region, the combustion is *non-premixed*. Conversely, when they are mixed together beforehand, the combustion is *premixed*. Finally, depending on the Reynolds number of the flow, defined in Eq. 1, combustion can be *laminar* or *turbulent*; and depending on the Mach number, defined in Eq. 2, combustion can be *subsonic* or *supersonic*. The Reynolds number is defined as:

$$Re_D = \frac{Kinetic\ energy}{Energy\ dissipation\ by\ viscous\ friction} = \frac{\rho u L}{\mu}, \tag{1}$$

where ρ is the fluid density (kg/m^3), u the flow speed (m/s), D a typical dimension (m), *e.g.* the inner diameter of a tube or the length of a flat plate, and μ the dynamic viscosity of the fluid (Pa·s). The Mach number is defined as:

$$M = \frac{Flow\ velocity}{Speed\ of\ sound} = \frac{u}{\sqrt{\gamma R_{specific} T_g}}, \tag{2}$$

where γ is the specific heat ratio, $R_{specific}$ the specific gas constant ($R_{specific} = R/M_g$ with $R = 8.314$ J.K^{-1}.mol^{-1} the universal gas constant and M_g the molar mass of

the gas), and T_g the ambient gas temperature.

2.1.2 Laminar premixed flames

In premixed combustion, an important parameter characterizing the combustible mixture is the equivalence ratio ϕ. It is defined by:

$$\phi = \frac{(\dot{m}_{Fuel}/\dot{m}_{Ox})}{(\dot{m}_{Fuel}/\dot{m}_{Ox})_{st}}, \tag{3}$$

where $\dot{m}_{Fuel}$ and $\dot{m}_{Ox}$ are the fuel and oxidizer mass flow rates, and "st" refers to the stoichiometric mixture, where the amounts of fuel and oxidizer are introduced such that no reactants remain at the end of the reaction. For $\phi > 1$, the mixture is known as rich, and lean for $\phi < 1$. A stoichiometric mixture has an equivalence ratio $\phi = 1$. For combustion in a static gas, the masses should be used instead of the mass flow rates in equation (3).

Laminar flames are interesting from a fundamental point of view because they allow for detailed comparisons between experiment, theory and computation. They are therefore widely used to validate chemical models, and can be considered as an "elementary building block" for more complex (*e.g.* turbulent) flames.

The structure of the premixed flame is schematically given in figure 1. The fresh gases ahead of the reaction front are heated by diffusion. When the gases reach the ignition temperature, the mixture starts to burn, as indicated in figure 1 by the chemical source term. The flame propagates as a combustion front in a direction opposite to the flow velocity.

The speed of the combustion front, called the laminar flame speed, can be expressed as [40]:

$$s_L \approx \frac{1}{\rho_u}\sqrt{\frac{\lambda_{therm} \cdot q_{chem}}{c_p}}, \tag{4}$$

where ρ_u is the density of the unburnt gas, λ_{therm} the thermal conductivity, q_{chem} the chemical reaction rate equal to the amount of mass burnt per unit volume and time, and c_p the specific heat of the gas mixture.

Laminar flame speeds depend on the fuel, the equivalence ratio, the temperature of the fresh gases and the pressure. To illustrate this, figure 2 from [41] shows the variations of laminar flame velocity with equivalence ratio for fuel-air mixtures

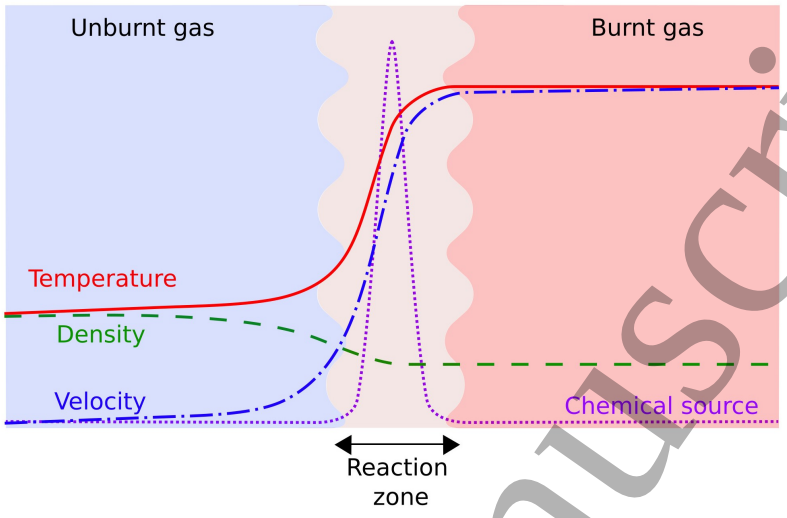

Figure 1: The structure of a stationary flame front in premixed combustion [39].

at an initial pressure of 1 atm and initial temperature of 298 K. It can be seen that for hydrocarbons, the speed is maximum slightly above stoichiometry, due to the maximal flame temperature at these conditions. Methane (CH_4) flames have a relatively lower maximal laminar speed at around 40 cm/s, compared to 73.5 cm/s for ethylene (C_2H_4) flames. Hydrogen (H_2) flames do not follow the same pattern as hydrocarbons, with a maximum flame speed of 325 cm/s at an equivalence ratio $\phi = 1.8$. This difference is caused by the significantly higher diffusion coefficient of hydrogen. Ammonia (NH_3) combustion, of significant recent interest because of the potential of a carbon neutral form of combustion as well as a potential carrier for hydrogen, have been added by the authors to the original plot. They have a maximal laminar flame velocity of around 7 cm/s [42]

These examples serve to illustrate the behaviors of different mixtures, but more variations based on initial pressure, temperature, dilution and mixing can also be expected. More information can be found in [34, 41].

2.1.3 Laminar non-premixed flames

If the reactants are initially separated, this is non-premixed combustion. In that case, heat and mass transfer are important as they take place on a scale comparable with the time scale of the reaction. For this reason, non-premixed combustion is also called "diffusion combustion". A typical example of a laminar non-premixed flame is

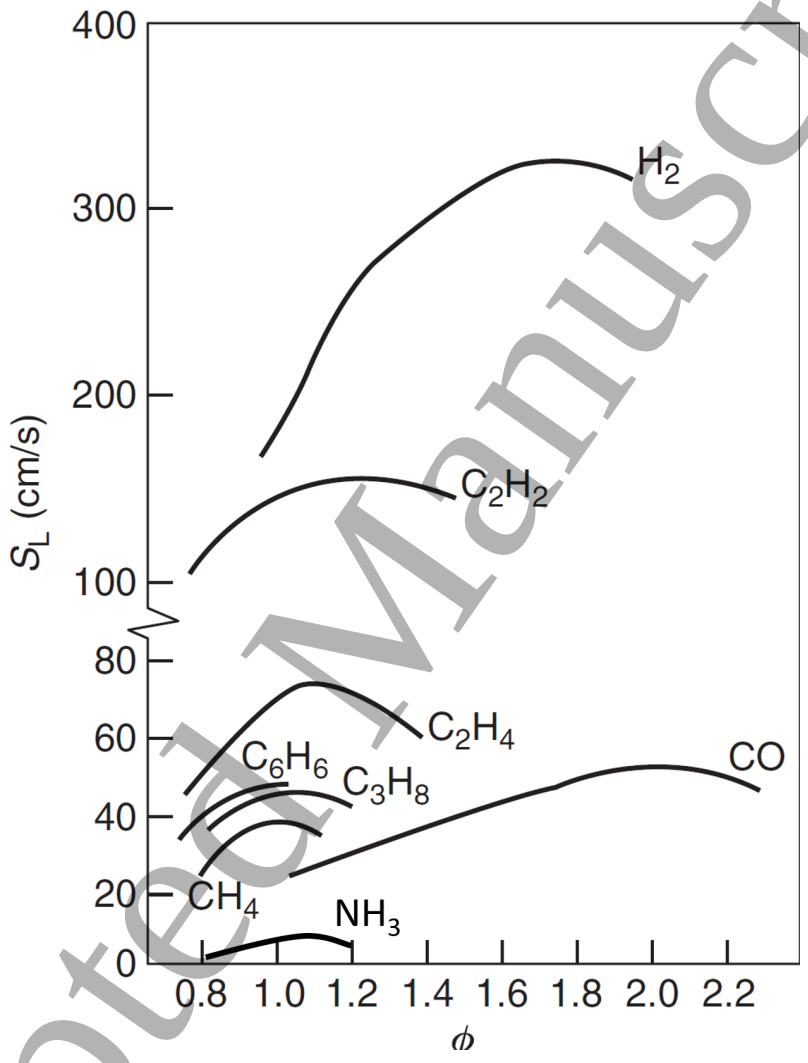

Figure 2: Variations of the laminar flame speed with equivalence ration ϕ for different fuel-air mixtures. Data measured at $P = 1$ atm a $T = 298$K. Original plot from [41]. Adapted to feature ammonia from [42].

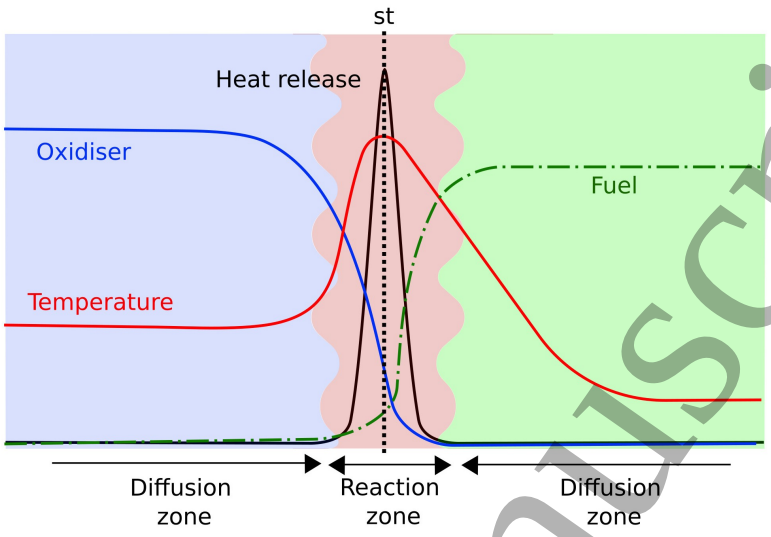

Figure 3: Structure of a laminar non-premixed (diffusion) flame.

a candle flame.

Figure 3 schematically illustrates the structure of a laminar non-premixed flame. The structure of the flame is completely different from the premixed case. Here, the oxidizer and the fuel are on opposite sides of the flame front and diffuse toward each other. Combustion reactions occur where the mixture approaches stoichiometry, with the burning rate governed by molecular diffusion of reactants toward the reaction zone. This type of flame is often studied in the laboratory using counterflow burners, where opposing, axisymmetric fuel and oxidizer jets mix at the stagnation plane.

2.1.4 Turbulent combustion

As indicated by equation (1), the Reynolds number represents a competition between the inertial forces (velocity of the flow) and viscous forces. When inertial forces much exceed viscous forces, the fluid flow is turbulent and characterized by the appearance of eddies of different sizes. In turbulent flows, the physical quantities fluctuate around their mean values, such that $X = \bar{X} + X'$, where $\bar{X}$ is the average quantity and X' the fluctuation. Fluctuations of velocity, temperature, gas density, pressure and concentrations can have a significant impact on the chemistry, either by influencing mixing or by leading to flame quenching.

To account for turbulence effects on combustion, dimensionless analysis is often conducted to compare the characteristic times of combustion kinetics and turbulence [34]. In combustion, the characteristic length is usually the flame thickness, noted δ_l, and the characteristic time is the ratio of flame thickness to laminar flame speed, s_L. In turbulence, characteristic scales range from the smallest to the largest eddies:

- the *integral* scale, corresponding to the largest eddies, is characterized by the integral length l_t and the velocity fluctuations $u'(l_t)$;
- the *Kolmogorov* scale, corresponding to the smallest eddies, is characterized by the Kolmogorov size l_k and the velocity fluctuations at Kolmogorov size, which correspond to the velocity of the smallest eddies: $u'(l_k) = u_k$.

The Damköhler number is defined on the largest turbulence scale as:

$$Da = \frac{Turbulence\ time}{Combustion\ time} = \frac{l_t/u'}{\delta_l/s_L}, \tag{5}$$

When $Da >> 1$, the combustion chemical time is smaller than the turbulence integral time. This corresponds to infinitely fast chemistry. In this case, turbulent motion can only wrinkle the flame front but does not affect its inner structure. When $Da << 1$, the combustion chemical time is larger than the turbulence integral time. In this case, reactants and products are mixed together instantaneously by turbulence. This limiting case corresponds to a perfectly stirred reactor (PSR) that can be modeled in 0D.

The Karlovitz number, Ka, is useful for the intermediate values of Damköhler ($Da > 1$). Ka is defined based on the smallest turbulence scale as:

$$Ka = \frac{Combustion\ time}{Kolmogorov\ time} = \frac{\delta_l/s_L}{l_k/u_k}, \tag{6}$$

The Ka number characterizes how the smallest eddies interact with the flame front. When $Ka < 1$, the flame is thinner than all turbulent scales and, as in the limiting case $Da >> 1$, there is no effect of the eddies on the inner structure of the flame front, only wrinkling. When $Ka > 1$, the analysis is complex, and several flame regimes are defined. More details can be found in [34]. This dimensionless analysis was first proposed by Borghi [43] and then completed by Peters [44]. It is usually represented in a Borghi-Peters diagram, such as the one presented in figure 4, to illustrate the various turbulent flame regimes. At high Ka, small eddies penetrate the flame front, thus thickening the flame. At low Ka, the wrinkled-flamelet regime is obtained. For intermediate values, the flame is both thickened and wrinkled. In all cases, the global fuel consumption rate per unit of flame area is increased compared

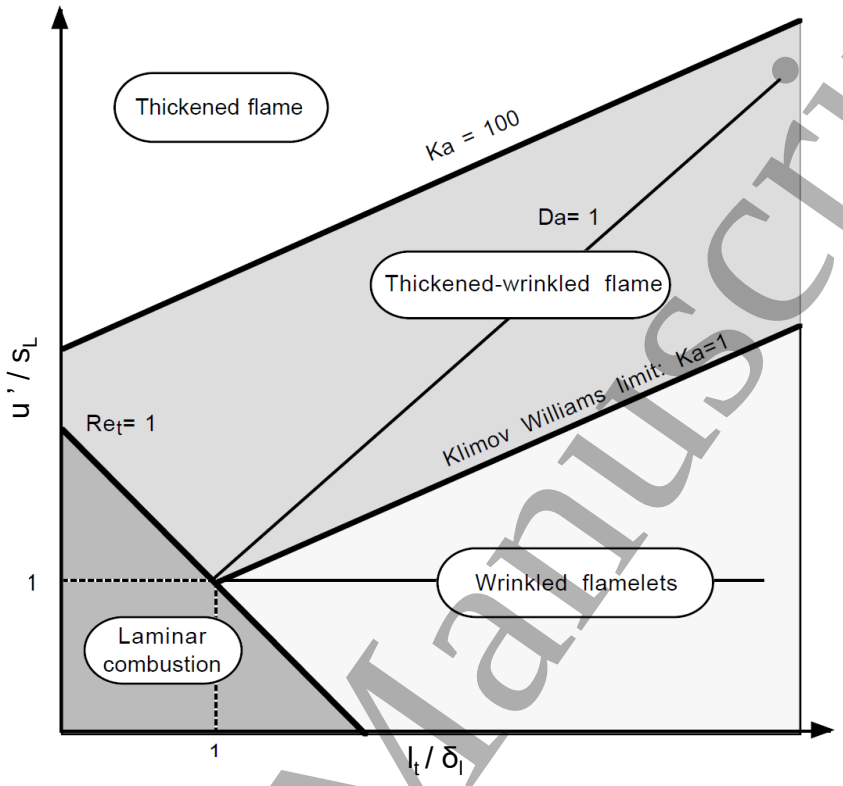

Figure 4: Turbulent combustion diagram (reproduced from [34]).

to the laminar flame. This classification in different turbulent flame regimes is useful for numerical simulations.

2.1.5 Supersonic combustion

At supersonic flow velocities (Mach number $M > 1$), convective transport dominates over diffusive transport owing to the high flow velocity. In a homogeneous combustion mixture, a self-sustained wave of exothermic chemical reactions propagates either as a subsonic deflagration or as a supersonic detonation wave [45], where flow dynamics and chemistry are tightly linked together. For premixed combustion waves, one should distinguish between subsonic and supersonic propagation. The former is referred to as the deflagration which is a near-constant pressure process. The latter is the detonation wave, through which the pressure increases 20 to 30 times in the reaction zone. Typical propagation velocities of detonation in gases are

on the order of 1 km/s, as compared to 0.1-100 m/s for deflagration. The detonation reaction zone has a cellular structure. It can be described as a set of Mach waves, with forward propagating shocks that result from the interaction of transversely propagating shocks, as described in [46] and the references therein. The elements of this structure are commonly referred to as detonation cells.

Fundamentals of supersonic combustion, deflagration and detonation physics would warrant their own review, and fall outside of the scope of this publication. Part 2 of this article [25] covers plasma-assisted supersonic combustion and detonation in greater detail. For the reader interested in learning more about the fundamentals of supersonic combustion, the authors recommend several alternate readings, from the most introductory on supersonic and hypersonic flows [47–49] to the more specific to combustion and detonation [34, 41, 45, 50].

2.2 Combustion chemistry

2.2.1 Basic principles of chemical kinetics

The concepts of global and elementary reactions are essential for understanding the kinetics of chemical processes. A global reaction, such as $2H_2+O_2 \rightarrow 2H_2O$ describes the overall process in one formula, presenting a "summary" of the full sequence of steps and ignoring intermediate species. The equation of an elementary reaction describes a single step in a chemical reaction that occurs in one interaction between molecules, atoms, electrons or ions. It reflects the actual number of particles involved in that specific step.

An elementary direct reaction between substances M_i and a reverse reaction between substances M_j with stoichiometric coefficients ν_i and ν'_j can be written as:

$$\sum_{i=1}^{N} \nu_i \mathrm{M_i} \underset{\mathrm{k_b}}{\overset{\mathrm{k_f}}{\rightleftharpoons}} \sum_{\mathrm{j}=1}^{\mathrm{N'}} \nu'_\mathrm{j} \mathrm{M_j} + Q, \tag{7}$$

where Q is the heat released/consumed in the reaction; Q is positive for exothermic reactions and negative for endothermic reactions. Equilibrium is established for a given ratio of the concentrations of reactants $[\mathrm{M}_i]$ and products $[\mathrm{M}_j]$ defined by the equilibrium constant K:

$$K = \left(\prod_{j=1}^{N'} \mathrm{M_j}^{\nu'_\mathrm{j}} \right) / \left(\prod_{i=1}^{N} \mathrm{M_i}^{\nu_\mathrm{i}} \right). \tag{8}$$

Elementary reactions occur in both directions, as indicated in equation (7) by the symbol "$\rightleftharpoons$" instead of a forward reaction arrow. The rate of the chemical reaction W is proportional to the product of concentrations of the reacting chemical species, each concentration raised to a power equal to the corresponding stoichiometric coefficient. The rates of the forward reaction, W_f, and backward reaction, W_b, are defined as:

$$W_f = k_f \prod_{i=1}^{N} \mathrm{M_i}^{\nu_\mathrm{i}}, \qquad W_b = k_b \prod_{j=1}^{N'} \mathrm{M_j}^{\nu'_\mathrm{i}}. \tag{9}$$

The coefficients k_f and k_b are the rate constants of the forward and backward reaction, respectively, and depend upon the gas temperature. The temperature dependence of a rate constant k is often expressed by the Arrhenius law:

$$k = \mathcal{A} T^b \cdot \exp\left(-\frac{E_a}{RT}\right), \tag{10}$$

where R is the universal gas constant, and E_a is the activation energy corresponding to an energy barrier to be overcome during the reaction to destroy or change the stable chemical bonds. The pre-exponential factor may have a weak temperature dependence. $\mathcal{A}$ and b are constants.

At equilibrium, the rates of the forward and the backward reactions are equal, $W_f = W_b$. The equilibrium constant K is a function of the gas temperature (see (10)) and can be expressed as the ratio of the rate constants of the forward and backward reactions:

$$K = k_f / k_b. \tag{11}$$

To be precise, deriving the equilibrium constant K should not rely solely on the kinetic equation, as uncertainty about whether we are dealing with the equation of a kinetic mechanism or an elementary reaction can lead to errors in the exponents of the rate expressions for the forward and reverse reactions. In general, a thermodynamic derivation of the equilibrium constant, based on the concept of chemical potential, is more rigorous and accurate [51]. A detailed discussion of thermodynamic principles, including the concept of chemical potential can be found in [52].

It should be noted that, whereas in equilibrium the system of ODEs reduces to a set of algebraic equations, in situations where chemical reaction kinetics and the temporal evolution of individual species are important, the full system of ODEs must be solved.

2.2.2 Ignition of a combustible mixture and limits of explosion

Let us consider the mechanism of combustion for the simplest case of a stoichiometric hydrogen–oxygen mixture, that is, a mixture with 2 molecules of hydrogen for every 1 molecule of oxygen. At relatively high temperatures and pressures, the kinetics of such a mixture are described by the branched chain mechanism [35, 53]:

$$H_2 + O_2 \xrightarrow{k_0} 2OH + 78 \text{ kJ/mole}, \text{ (chain initiation)} \quad (12)$$

$$H + O_2 \xrightarrow{k_1} OH + O + 70 \text{ kJ/mole}, \text{ (chain branching)} \quad (13)$$

$$O + H_2 \xrightarrow{k_2} OH + H + 8 \text{ kJ/mole}, \text{ (chain branching)} \quad (14)$$

$$OH + H_2 \xrightarrow{k_3} H_2O + H - 62 \text{ kJ/mole}, \text{ (chain development)} \quad (15)$$

$$H \xrightarrow{k_4} 1/2H_2 \text{ (chain termination, walls)} \quad (16)$$

$$H + O_2 + M \xrightarrow{k_5} HO_2 + M - 203 \text{ kJ/mole}, \text{ (chain termination, volume)} \quad (17)$$

Here reaction (12) is a reaction of chain initiation under conditions of autoignition. Reactions (13) – (15) are responsible for chain prolongation, with or without branching. Linear chain reactions are the reactions in which one radical reacts with a stable component of the and produces exactly one new radical (reaction (15)), keeping the total number of radicals constant. In branched chain reactions, the number of radicals formed exceeds the number consumed (reactions (13) – (14)), leading to an exponential increase in the concentration of active species. Nonlinear chain reactions (non considered here) involve reactions between two radicals, leading to their mutual consumption or transformation. Reactions (16) – (17) are the reactions of chain termination.

It should be noted that even the simplest mechanism of H_2:O_2 combustion can include, according to different authors, at least $9 - 19$ elementary steps [54]. An alternative mechanism comprising 11 reactions, including nonlinear chain reactions, can be found in [55]. The elementary steps of these mechanisms are always reactions of H_2 and O_2 dissociation followed by a set of reactions involving O, H, OH, HO_2,

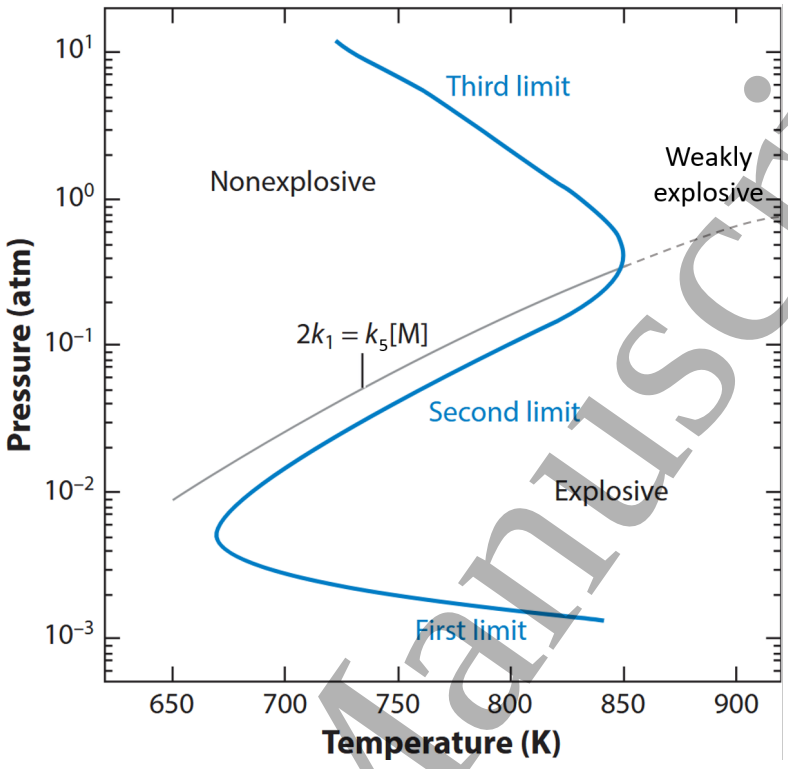

Figure 5: Limits of explosion for hydrogen–oxygen mixture (adapted from [38, 56]). Rate constants k_1 and k_5 correspond to equations (13) and (17) respectively (see text). The extended second limit is designated by a dashed line (see text).

and, at lower temperatures, H_2O_2.

The ignition delay is defined as the time period between the start of the process, i.e. heating or mixing of gases, and the time of an abrupt increase in temperature, pressure, emission intensity, and rate of chemical reactions. During this so-called induction period, the density of radicals increases but the fuel is practically unconsumed and the heat release is negligibly low. Above a certain radical concentration, there occurs a rapid change in temperature and density of the main and intermediate chemical species that leads to ignition of the gas mixture.

Figure 5 illustrates critical ignition parameters. The non-monotonic Z-shape curve represents the so-called limits of autoignition, or explosion limits, separating zones where the mixture is explosive (to the right of the curve) or nonexplosive

(to the left of the curve). Numerous studies over several decades [41, 51, 55, 57–59] have been devoted to the analytical and numerical analysis of these explosion limits. A detailed mathematical description of the limits is given in [57]. The sensitivity analysis provided in [59] clearly illustrates that the first ignition limit is governed by the balance of atomic hydrogen: reaction (13) dominates the chain propagation, while the loss of hydrogen atoms is primarily due to diffusion and recombination on the walls at low pressures, reaction (16). The second explosion limit is caused by a competition between two reactions in volume: the same chain branching reaction (13) and a reaction (17) producing hydroperoxyl radical HO_2. The hydroperoxyl radical is relatively unreactive so that it is able to diffuse to the wall. The line in the figure 5 is the solution of system of equations (13)-(17) in assumption of quasistationary concentrations [38], $2k_1 = k_5 M$. Some authors plot the equal rates only for two reactions, (13) and (17), as an estimate for the second limit. The third explosion limit is due to a reaction that overtakes the stability of the HO_2, the reaction suggested in [41] is HO_2+$H_2 \rightarrow H_2O_2$ +H. With the ensuing dissociation of hydrogen peroxide into two OH radicals, highly reactive chain carriers, the continuation of the combustion chain is possible. On the contrary, a slow destruction of H_2O_2 on the wall stops the chemical chain. The exact position of the third limit is highly sensitive to the non-linear reactions, as shown in [55].

A distinctive effect is observed at high pressures and temperatures. In the literature, this phenomenon is referred to as the extended second (kinetic) limit, the details can be found in [41, 58]. This limit is schematically shown with a grey dashed curve in figure 5. In the case of a fast adiabatic experiment (for example, after the reflected shock wave), the kinetic balance between the reactions (13) and (17) provides the boundary between two modes of combustion: localized ignition kernels are observed in a weakly explosive region at high pressures and temperatures, while a strong homogeneous explosion is observed below the curve.

Finally, change of explosion limits under artificial additions of radicals was already considered theoretically in the pioneering books of Semenov [51, 60], published in the 1950s. The Russian and English versions are referenced here, with the former being more complete. Modern numerical analysis of this problem [56] can be key for plasma-assisted combustion kinetics.

2.2.3 Kinetic mechanisms for hydrocarbon combustion: methane mechanisms as example

Building combustion mechanisms is a large–scale thorough task including analysis of available experimental and theoretical data, composing the mechanism itself, performing detailed sensitivity analysis and validation of the mechanism on the basis of the experimental results. Unlike in plasma science, "standard" combustion mechanisms for many different fuels have been developed and accepted by the community. These mechanisms are thoroughly validated on available experimental data. Even though different and complex kinetic mechanisms exist for many fuels, the availability of kinetic mechanisms is discussed below using methane as an example.

Petersen *et al.* [61] presents one of already classical examples of validation of the first widely accepted GRI–Mech 1.2 mechanism [62] developed under support of the Gas Research Institute. This mechanism describes the ignition of CH_4 at high temperatures. It includes 175 elementary reactions and 32 species. The validation covers a wide range of experimental conditions from shock tube measurements: $T = 1505 - 2043$ K, $P = 9.4 - 86.8$ atm, equivalence ratios $\phi = 0.5 - 4.0$. In shock tube experiments, the combustible mixtures are highly diluted, typically using Ar or N_2 as inert diluent. In the mentioned experiments, the concentration of Ar or N_2 in the mixture varied from 90% to 99.61%. Although GRI–Mech 1.2 (and later the modified GRI–Mech 3.0 [63]) mechanism described ignition delay times and flame velocities for a wide range of experimental parameters, it significantly overestimated the ignition delay time for rich mixtures at high pressures ($P > 40$ atm) and low temperatures ($T < 1300$ K). To correct this limitation, the RAMEC (RAM accelerator MEChanism) mechanism was developed [64]. In all, 13 reactions and 6 species were added to the original GRI–Mech 1.2 model. Most of the new reactions in RAMEC were taken from low temperature methane oxidation mechanisms. Although they include more than 30 species, both GRI–Mech and RAMEC describe high–temperature oxidation of methane and were not developed and tested for the chemistry of higher hydrocarbons.

For combustion mechanisms of complex hydrocarbons and fuel blends, we refer the reader to a series of papers [65–67] from the Combustion Chemistry Center (CCC) [68]. These were the first studies to present ignition delay times for a wide range of conditions obtained in shock tubes and rapid compression machines (RCM). Typically, shock tubes provide high temperatures (thousands of K) and relatively low pressures (units of atm), while RCMs can operate at low initial temperatures ($700 - 1000$ K) and very high initial pressures (tens–hundreds of atm).

Taking into account the increasing performance of numerical modeling of combustion, linking together detailed kinetics and complex hydrodynamics, a deep analysis of available kinetic mechanisms is of paramount importance. Two recent papers [69, 70] compare the performance and efficiency of about 10 methane combustion mechanisms for different conditions. In [69], thirteen CH_4 combustion mechanisms were tested against the experimental data on ignition delay times, obtained in shock tubes and RCM. The tested mixtures include oxygen, a diluent (N_2, Ar, He, CO_2, or H_2O), and pure methane or blends of CH_4 with H_2 and/or CO. The performance of each mechanism was investigated in various ranges of temperature, pressure, equivalence ratio, and diluent ratio. Four mechanisms, Aramco-II-2016 [71], Caltech-2015 [72], Glarborg-2018 [73], and SanDiego-2014 [74], proved to generally best reproduce the experimental data, but the authors of [69] underscore that there is no unique solution for all ranges of parameters, and if an accurate methane combustion mechanism is needed under a specific range of conditions, it can be selected based on the detailed analysis provided in [70]. Similarly, twelve methane combustion mechanisms were tested in [70] against a large amount of experimental data on laminar burning velocities of methane:oxygen:diluent mixtures (with additions of H_2/CO) covering a wide range of equivalence ratios, diluent ratios, cold side temperatures and pressures. The diluents included N_2, H_2O, CO_2, Ar and He. The authors of [70] recommend mechanisms FFCM-I-2016 [75], SanDiego-2014 [74], and NUIG1.1-2021 [76] for engine simulations. The Aramco-II-2016 [71], Konnov-2009 [77], Caltech-2015 [72] and Glarborg-2018 [73] mechanisms have the lowest average errors for the reproduction of all available methane laminar burning velocity data. The references [69, 70] provide excellent examples of the analysis of kinetic mechanisms prior to their application. They also demonstrate that no universal solution exists; each kinetic mechanism must be selected based on the specific conditions for which it was developed. Note that kinetic mechanisms must be selected based on the parameters to reproduce: a mechanism reproducing laminar burning velocity or ignition delay time, does not necessarily reproduce density of minor species. This fact is discussed in [14] on example of CH_4:O_2=2:1 mixture for two different mechanisms calculating, for autoignition and for simplified plasma-related conditions, the ignition delay time and kinetic curves of formaldehyde.

In the above subsection, methane combustion was used as an illustrative example to describe the construction and analysis of combustion mechanisms. As already noted, kinetic mechanisms for heavier hydrocarbons are considerably more complex [68]. Recent trends toward generalized modeling in the field of low-temperature

chemistry (LTC) of heavy hydrocarbons [78] provide opportunities for broader treatment and unification of combustion and plasma kinetics [79]. Reference [78] suggests a strategy to accurately capture the chemical kinetics of real fuels in both the LTC and negative temperature coefficient (NTC) regimes, using a set of compact, fuel-specific reactions but providing the most general trends. The NTC region signifies a temperature range in which the overall reaction rate decreases with increasing temperature, a characteristic feature of heavy hydrocarbon combustion at $T < 1000$ K. The same paper underlines that, in the low-temperature regime, a fuel first undergoes partial oxidation (first-stage ignition) to produce intermediate species (e.g., CO, CH_2O), accompanied by modest heat release. The associated temperature rise can push the reaction to the intermediate temperature/NTC regime, where the chemistry of radicals such as OH and HO_2 then controls the overall oxidation (second-stage ignition). A finite induction period separates the first- and second-stage ignition. This approach opens the door for linking plasma chemistry with combustion chemistry. For example, paper [80] shows, by numerical modeling, the disappearance of the NTC zone in propane under the action of non-equilibrium plasma.

2.3 On numerical modeling of combustion

Numerical combustion is now essential for both academic research and industrial applications. For researchers, it provides comprehensive data and insights into combustion phenomena that cannot be obtained experimentally. In industry, simulations are progressively replacing experiments for the development of new combustion systems, offering flexibility and cost savings. However, these simulations must account for the broad range of temporal (from 10^{-9} s to 1 s) and spatial scales (from 10^{-6} m to 1 m) in combustion processes. From a 0D Perfectly Stirred Reactor (PSR) simulation with only kinetics to the 3D turbulent simulation of a combustion chamber, the toolkit for numerical combustion is wide. A summary of the existing methods and approaches is provided in the following section.

2.3.1 Chemical models

The detailed kinetic mechanisms presented in the previous section represent the state-of-the-art in combustion chemistry, with many intermediate reactions and species. The GRI–Mech for CH_4, which is the simplest carbonated fuel, already comprises of 32 species and 175 reactions, meaning that at each time step, a 32x32 nonlinear system must be solved. The more complex the fuel, the larger the kinetic mechanism. To reduce complexity, several methods were developed in the past decades: mechanism reduction, tabulated chemistry, and optimized chemistry. An overview

of these methods is given in [81].

2.3.2 Turbulent flows

To consider the effects of turbulence, which are key in most real combustion systems, 3D simulations are needed. Several approaches can be used for turbulence simulations: Direct Numerical Simulation (DNS), Reynolds Average Navier-Stokes (RANS) and Large Eddy Simulation (LES). DNS is the most detailed, capturing all turbulence scales, while RANS simulates the main flow and models all turbulent effects. LES offers a middle ground, simulating larger turbulence scales and using a simplified model for the smaller ones. For LES and RANS, since the turbulence is partially or totally modeled, the interactions between combustion and turbulent eddies must be modeled as well. Detailed recommendations and a wide variety of approaches are presented in [34, 82]. Depending on the problem, the desired level of fidelity, and the available computational resources, a trade-off between turbulence and combustion models must be made.

The limitations of transient and multidimensional combustion modeling are twofold: (i) closure of source terms in the transport equations for chemical species and energy that appear in RANS (ensemble-averaged) and LES (filtered-average) governing equations; (ii) integration of transport equations for a large number of chemical species that are typically involved in combustion, especially with large hydrocarbon molecules.

Depending on the combustion regime, various modeling strategies have been developed to overcome these challenges and allow the inclusion of tens or even hundreds of species, even in engineering-scale simulations with complex geometries and realistic fuels (kerosene, diesel, gasoline, etc.), where RANS or LES are commonly used with a chemistry that involves a large number of species. For instance, LES with chemistry tabulation methods (applied to both premixed and non-premixed flames) have been well developed and are currently widely used for daily combustion modeling in engineering combustors. In these approaches, instead of directly solving transport equations for all species, the thermodynamic state of the CFD cells at each location and time is obtained based on a precomputed lookup table where thermodynamic state and/or source terms are stored on a very low-dimensional manifold with very few table entries, e.g., progress variable, mixture fractions, etc...

Examples are flamelet models wherein the thermodynamic state of the mixture can be mapped onto a low-dimensional manifold—typically defined by progress variables and/or mixture fractions. Recent works lift some of the limitations with the extremely low-dimensional manifold of flamelet-based models, especially for partially

premixed combustion [83] or combustion involving local or global extinction [84].

2.3.3 Challenges for plasma integration into combustion modeling

The temporal and length scales of plasma phenomena can be several orders of magnitude lower than those of combustion. Additionally, plasma kinetics are more complex than combustion kinetics, with many more species and reactions. The coupling of plasma and combustion thus increases the stiffness of the mechanisms and greatly increases the complexity of the mesh and the computational cost. Significant improvement in this coupling have been made in recent years, which is discussed in Part 2 of the article.

3 Plasma

3.1 Plasma: main definitions and parameters

3.1.1 General considerations

This section aims to provide a general understanding of the key properties and concepts of weakly ionized plasma physics to allow combustion specialists to grasp the phenomenology of typical laboratory plasmas. This section is in no way an exhaustive fundamental review and the authors encourage the readers to turn to more detailed discussions on these topics, as can be found in the books [85–91] and others should they require it. In the most general definition, a plasma is a quasi-neutral medium of charged particles.

One of the fundamental properties of a plasma is its temperatures. In the plasma physics field, the electron temperature is commonly measured in electronvolts (eV). The conversion factor from eV to K is given by equating the energy gained by an electron accelerated by a potential difference of $U = 1$ V to the characteristic thermal energy kT such that:

$$T = \frac{e}{k} = 11610 \text{ K} \tag{18}$$

The use of plural for temperature in the previous paragraph was intentional. Indeed, in a plasma, the temperatures of different species ($e.g$ heavy neutral particles, ions and electrons) are not necessarily equal. This is addressed further into the text (see Sec. 3.1.3).

This discussion about the properties of plasma will begin with the definition of a key parameter at the cornerstone of plasma physics: the Debye length. The Debye

length or Debye–Hückel screening length r_D is the distance over which the electric field of a single charge extends in a medium containing free positively and negatively charged particles. Outside the Debye sphere (sphere of radius equal to the Debye length), the electric field is shielded as a result of polarization of the medium. The Debye length can be obtained from the Poisson equation and Boltzmann distributions of charged particles, and is expressed (in SI system) in the following way:

$$r_D = \sqrt{\frac{\varepsilon_0 k T_e}{n_e e^2}}, \tag{19}$$

where ε_0 represents the vacuum permittivity, k the Boltzmann constant, T_e the temperature of electrons, n_e the electron density, and e the electron charge.

As previously mentioned, some plasmas have very different ion and electron temperatures, $T_e \gg T_i$. In general, r_D is a function of both these temperatures. But in some particular cases, it can be assumed that ions, being much colder and slower than electrons, are "immobile"; the redistribution of charge is determined by electron motion only [85, 91] and can still be estimated using equation (19).

To provide some characteristic values, for a plasma with electron density $n_e = 10^{14} - 10^{15}$ cm^{-3} and electron temperature $T_e \approx 3$ eV, typical for streamer discharges at atmospheric pressure, the Debye radius is below 1 micrometer.

If the characteristic size of the system greatly exceeds the Debye radius, the plasma is quasi-neutral. For a large total number of charged particles N_D in the Debye sphere, the plasma is referred to as ideal. This is described by the following equation:

$$N_D = \frac{4\pi}{3} r_D^3 n_e \gg 1, \tag{20}$$

In such cases, the Coulomb interaction energy is much smaller than the kinetic energy. Otherwise, the plasma is known as non-ideal. Combining equations (19) and (20) for an electron temperature $T_e \approx 3$ eV, the electron density at which the Coulomb interactions should be taken into account is roughly $n_e > 10^{18} - 10^{19}$ cm^{-3}. This range falls outside the scope of this work and will not be discussed further here.

3.1.2 Plasma parameters observed in nature and in laboratory

Figure 6 provides a general overview of plasma parameters observed in nature and in laboratory conditions. Three categories can be considered depending on the charged-particle density and temperature: relativistic, quantum and classical plasmas.

Relativistic plasmas (*e.g.* external shell of a neutron star) are characterized by very high temperatures, on the order of the rest energy of an electron ($T \geq m_e c^2 =$

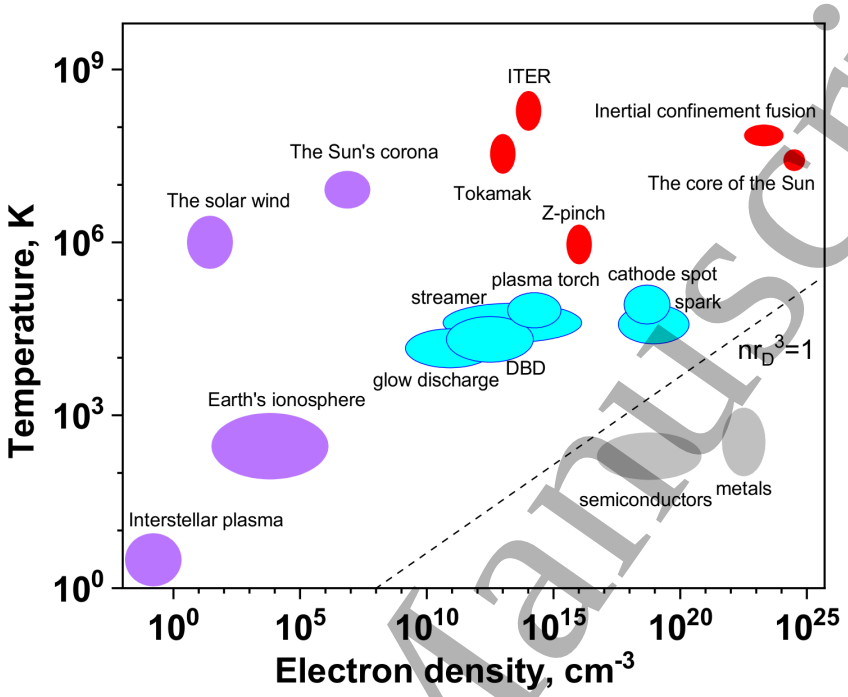

Figure 6: Plasma parameters in the universe. Space plasmas (violet), low temperature plasmas (blue), fusion plasma, (red), and solid state objects (grey). The dashed line is the boundary between ideal (above the line) and non-ideal plasmas. [86–88,92]

500 keV). These temperatures, on the upper limit of plasma conditions, will not be described here.

For quantum plasmas, a mathematical apparatus taking into account strong electron-ion interactions is required. It characterizes the phenomena occurring at extremely high electron densities ($10^{18} - 10^{24}$ cm^{-3}) and low temperatures (hundreds of K). These conditions are found in semi-conductors, metals, or metal-ammonia solutions. They will not be covered here either.

This leaves classical plasmas, which are of interest to us. This broad term encapsulates dozens of orders of magnitude in electron number densities and temperatures. They can be further categorized as follows.

A first category corresponds to **high-temperature**, or **fusion plasmas**. For example, the temperature in the center of the Sun is around 10^7 K, and the density of charged particles far exceeds the density of electrons in metals (and by several orders

of magnitude). Controlled thermonuclear fusion reactors are expected to produce plasmas with temperatures of similar order if not higher (the expected temperature in ITER is around $1.5 \cdot 10^8$ K).

Space plasmas are characterized by their low electron densities. In the Earth's ionosphere, the electron density varies from 10^2 cm^{-3} in the D-region at $60-90$ km to $10^5 - 10^6$ cm^{-3} in the F–region at altitudes of hundreds of kilometers. In the same region, the temperature does not exceed a fraction of an electronvolt (or $T = 10^2$ K). In the solar corona, the electron density can reach 10^8 cm^{-3} with accompanying temperatures of 10^6 K. However, the solar photosphere (the outermost visible layer of the Sun, closer to the center than the corona) has a charged particle density of $10^{15} - 10^{16}$ cm^{-3} and a temperature of roughly 6000 K.

Finally, plasmas with electron density 10^9 cm$^{-3} < n_e < 10^{18}$ cm^{-3} and temperatures $T < 10^5 - 10^6$ K are typically known as **low temperature plasmas**. This range covers atmospheric plasma phenomena (*e.g.* lightning and high-altitude lightning) but also most laboratory plasmas and their numerous applications. Going further, only this range of parameters will be discussed.

3.1.3 Low temperature plasma, equilibrium and nonequilibrium plasma

3.1.3.1 Electron temperature and reduced electric field

In most cases, the term low temperature plasma is used to refer to gas discharges. While there has been a growing interest in the field of plasma in liquids [93], this article will limit its consideration to gas media.

Many technological achievements in the 20^{th} century can be attributed to applications of low temperature plasmas, most of all in the field of microelectronics [91]. These plasmas are still intensely researched today, and potential applications are still being studied [5, 6]. Some of the recent fields that have seen developments are additive manufacturing (AM) and coating, atomic layer etching (ALE) and deposition, electrification of chemical conversion, medical applications and pollution control.

As mentioned previously, low temperature plasmas can be either equilibrium or nonequilibrium. This definition establishes the relationship between the temperatures of the different plasma subsystems. It can be seen as the balance of energy (or temperature) between the different components. For example, an electron accelerates (gains energy) by an electric field, and transfers this energy to other particles through collisions. The balance between each subsystem will depend on the efficiency of the energy exchange process. For an equilibrium plasma, the temperatures of all subsystems are equal:

$$T = T_i = T_e \tag{21}$$

Conversely, when there is no equality between individual ensembles of particles or degrees of freedom, the plasma is in nonequilibrium:

$$T << T_i << T_e \tag{22}$$

It should be noted that when considering low temperature nonequilibrium plasma, the temperature on the ordinate axis in Figure 6 is the temperature of electrons. The gas temperature can be significantly lower.

Given that plasma-assisted combustion involves chemically reacting gas mixtures with internal degrees of freedom, the concept of equilibrium becomes nontrivial. Several considerations regarding this issue are discussed later in subsection 3.2.6.

Under laboratory conditions, the most common method of producing plasma is a gas discharge. This is defined as the production of charged species in a discharge-gap filled with a certain gas mixture. Applying a potential difference between the electrodes leads to ionization in the gap. When the discharge gap is closing and conductive current starts to flow between the electrodes, the process of closing of the gap is called "gas breakdown". This description leads to a semantic discussion over the use of the term "plasma discharge". While sometimes used in the plasma community, the authors suggest that this term would be less accurate than others such as "gas discharge plasma" or "discharge induced plasma". Indeed, a plasma (ionized gas) is the result of a discharge.

When a potential difference is applied between the electrodes, seed electrons in the gap are accelerated and can collide with heavy particles to produce additional electrons. This is called electron-impact ionization. It is often the main source of production of secondary electrons and positive ions. Characteristic ionization energies are on the order of 10 eV or higher as shown in Table 1 for a few atoms and molecules. The exception is the alkali metals, which have a very low ionization threshold (3.89 eV for Cs or 5.39 eV for Li [94]), but these elements are beyond the scope of this review. In most discharges, the average electron energy does not usually exceed a few eV, which means that ionization is due to electrons with higher than average energy, or from the “tail” of the electron energy distribution (see section (3.2.1)).

The average electron energy in a gas $\langle\epsilon\rangle$, or electron temperature T_e, is a function of the reduced electric field:

$$\langle\epsilon\rangle = \mathcal{F}(E/N). \tag{23}$$

Table 1: Ionization energy for selected atoms and molecules

Species	Ionization energy (eV)	References
O_2	12.07	[94]
O	13.62	[94, 95]
H_2	15.43	[94]
H	13.60	[94]
CH_4	12.98	[94]
NH_3	10.16	[94, 96]
N_2	15.58	[94]
N	14.53	[94, 97]
Ar	15.76	[94]
He	24.59	[98]
H_2O	12.61	[94]
CO_2	13.79	[94]

where E is the electric field and N is the gas number density (or density of particles that participate in collisions). It is important to note that in many textbooks on low temperature plasma physics, the reduced electric field can be represented as E/P, with P the gas pressure. Most experimental data are obtained at room temperature, which implicitly assumes the established relation $P = NkT$ at $T \approx 300$ K. E/N is a more physically meaningful quantity for plasma-assisted combustion. This reduced electric field is usually measured in Townsend (Td), a non-standard unit. For reference, 1 Td $= 10^{-17}$ V·cm^2.

3.1.3.2 Swarm parameters and similarity parameters

Another set of key parameters in gas discharges are the "swarm parameters" [99], sometimes referred to as transport coefficients [100]. As defined in a review by Petrovich *et al.* [101], a swarm denotes an ensemble of charged particles moving through a background gas under the influence of an external electrostatic force. The charge density should be low enough that is does not influence the electric field and Coulomb interactions between charged particles are negligible. Swarms can be considered as the low-current limit of gas discharges, and consequently, the obtained data (*e.g.* [102, 103]) are suitable for normalizing scattering cross-sections and validating collisional aspects of plasma models. Focusing solely on the swarm

parameters for electrons (ion swarm parameters are beyond the scope of this article), typical quantities of interest include the drift velocity, the longitudinal and transverse diffusion coefficients (with respect to the direction of the electric field $\mathbf{E}$), the first Townsend ionization coefficient, and attachment coefficients (which describe the loss of electrons due to formation of negative ions).

The drift velocity v_{dr} represents the average velocity of electrons in the opposite direction of electric field and is typically much lower than the thermal velocity. The electron mobility μ denotes the proportionality coefficient between the drift velocity and the electric field,

$$\mathbf{v}_{dr} = \mu(E/N)\mathbf{E}. \tag{24}$$

It should be noted that μ depends on the reduced electric field. This dependence arises because the mobility is determined by the electron energy distribution function , which in turn is controlled by E/N. A detailed discussion of the EEDF and its role in description of low temperature plasma is given in the next section. In practice, the mobility can be calculated or obtained from swarm experiments. A comparison of calculated and measured mobility is a typical validation test for the selected set of cross-sections of electron impact reactions. For practical applications, the dependence of electron mobility on the reduced electric field can be neglected. For example, in air μ decreases by less than a factor of two as E/N increases from 100 to 1000 Td, which justifies the use of equation (24) under the assumption of constant mobility over a broad range of reduced electric fields.

In gas discharge physics, two Townsend coefficients are distinguished. They are empirically derived parameters that describe development of a discharge in a given gas mixture under a specified electric field. The first Townsend coefficient, α_i, characterizes electron multiplication in a gas and is among the most frequently measured swarm parameters. The second Townsend coefficient quantifies the electron yield from the cathode under bombardment by positive ions. From basic considerations of the probability that an electron travels a certain distance without collisions and undergoes ionization at energies above the threshold [85, 104], one can obtain the following expression for the first Townsend coefficient:

$$\frac{\alpha_i}{N} = \mathcal{A} \cdot \exp\left(-\frac{\mathcal{B}}{E/N}\right) \tag{25}$$

Here, $\mathcal{A}$ and $\mathcal{B}$ are empirical constants, N is the gas density

Combining the first ionization coefficient α_i with the condition for a self-sustained Townsend glow discharge yields one of the best-known similarity laws in gas discharge

physics. Although steady Townsend discharges are not used in plasma-assisted ignition, this example illustrates the role of similarity laws. In plasma physics, the onset of a discharge is usually termed "ignition" or "breakdown"; here we avoid the former (except in this paragraph) and note that the latter can also describe ionization front propagation. The "breakdown voltage" is defined as the voltage at which plasma ignites under an infinitely slow increase of the applied voltage across the gap, with other parameters fixed. A self-sustained Townsend discharge arises when an initial electron, accelerated in the electric field, traverses the electrode gap and produces secondary electrons by impact ionization, while the resulting positive ions return to the cathode and, through secondary emission, release at least one new electron, thereby closing the cycle. Incorporating α_i into this condition gives the Paschen curve, which relates the breakdown voltage to the product pd, where p is the gas pressure (effectively the gas density) and d the electrode spacing. For each gas, the breakdown voltage decreases with increasing pd, reaches a minimum, and then rises again (see figure 7). Here, pd serves as a similarity parameter: over a broad density range, the breakdown voltage remains constant if pd is preserved.

Paschen's law, derived for a static breakdown voltage, separates the region between "no discharge" (below the curve) from the region of "Townsend discharge" (above the curve). The Townsend mechanism describes a glow discharge, when sepa-

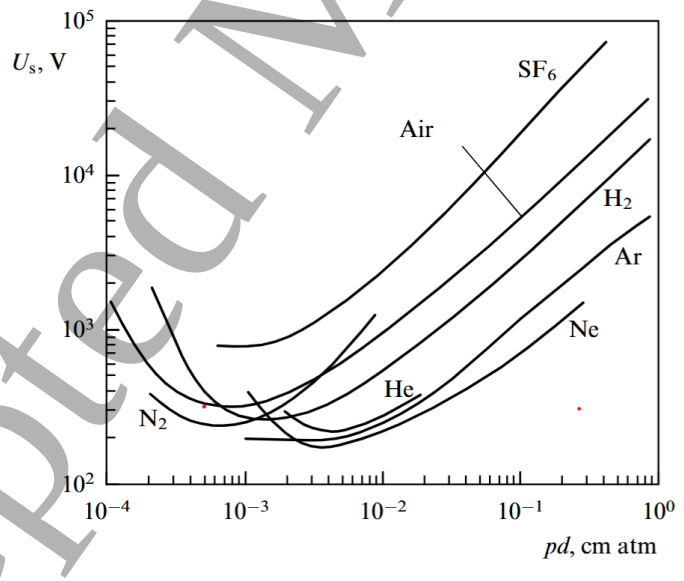

Figure 7: Breakdown voltage versus the product pd for different gases (Paschen curves), [104]

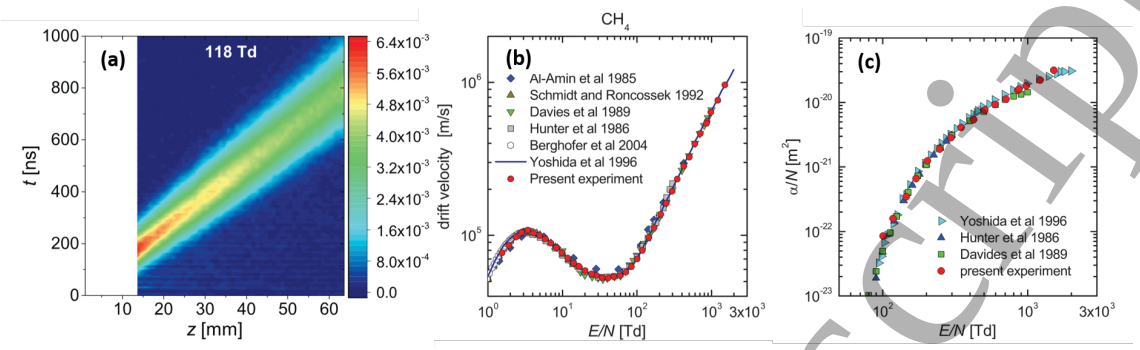

Figure 8: Swarm parameters: (a) swarm maps recorded in methane, for E/N = 118 Td. The color scales represent electron density and are given in arbitrary units; (b) drift velocity and (c) reduced effective ionization coefficient. Reproduced from [100]. Previous data: Al-Amin et al [106], Schmidt and Roncossek [107], Davies et al [108], Hunter et al [109], Berghöfer et al [110], Yoshida et al [111]

rate electron avalanches provide a uniform pattern. In the case of pulsed voltage, the situation changes. Streamer mechanism of breakdown dominates when the electric field in the head of a single avalanche becomes comparable to the external electric field. The modified Pachen's law should take into account an overvoltage (percent of voltage above a static breakdown threshold) as a function of pd. More details about triggering and development of pulsed discharges can be found elsewhere [105].

Similarity laws are crucial because they allow complex discharge behaviors to be described using universal parameters, enabling predictions across different conditions. They simplify analysis by linking various discharge characteristics through consistent relationships, but are valid only when the underlying discharge processes remain unchanged. The reference [104] provides a discussion on applying the similarity laws to pulsed discharges, and consider, together with classical combination of parameters, like pd, α_i/p etc., parameters including the charge formation time.

Coming back to discussion on the swarm parameters, measured excitation coefficients of individual internal states and the characteristic energy (ratio of diffusion coefficient to mobility) can also be considered as swarm parameters in the case of an equilibrium energy distribution of electrons.

New generation drift tubes, namely scanning drift tubes [100, 103], are capable of mapping the complete spatio-temporal evolution of electron swarms, developing between two plane electrodes ("swarm maps"). These systems operate with electron swarms initiated by photoelectron pulses; the spatio-temporal distribution of the electron flux is recorded at a fixed electric field and gas density, while the electrode

gap length is varied. Scanning of swarm parameters across a wide range is possible in a very short time (on the order of tens of minutes). Figure 8 [100] presents (a) an example of raw data: (b) drift velocity and (c) reduced effective ionization coefficient for methane. The results reported in [100] demonstrate excellent consistency with the data obtained in earlier classical swarm parameter measurements.

Swarm parameters are very important for validation of a set of cross-sections when calculating the electron energy distribution function (see sections (3.2.1,3.2.2)).

3.2 Plasma chemistry

3.2.1 Boltzmann equation and the electron energy distribution function

To describe the behavior of electrons in plasma and the plasma chemistry related to collisions with electrons, it is necessary to introduce the concept of the electron distribution function. The velocity distribution function of electrons, $f(\mathbf{r}, \mathbf{v}, t)$, or often the electron energy distribution function, EEDF, can be found by solving the Boltzmann kinetic equation [85, 112–114]. The Boltzmann equation is, in essence, a balance equation for the number of electrons $f d\mathbf{r} d\mathbf{v}$ in an elementary volume n an elementary volume defined by spatial coordinates and velocities. The equation takes into account electron motion in the electric field and collisional processes in the plasma. Mathematically, it is expressed by:

$$\frac{\partial f}{\partial t} + \mathbf{v} \cdot \nabla f + \frac{\mathbf{F}}{m_e} \cdot \nabla_v f = \left(\frac{\partial f}{\partial t} \right)_{col} \tag{26}$$

where f is the distribution function, $\mathbf{v}$ is the electron velocity vector, $\mathbf{F}$ is the external electric field, and m_e is the electron mass. The collision term on the right hand side of the Boltzmann equation comprises all kinds of binary collisions with electrons. It accounts for the elastic S_{en}^{el} and inelastic S_{en}^{inel} electron collisions with neutral atoms and molecules, and, if necessary, electron-ion S_{ei} and electron-electron S_{ee} collisions:

$$\left(\frac{\partial f}{\partial t} \right)_{col} = S_{en}^{el} + S_{en}^{inel} + S_{ei} + S_{ee}. \tag{27}$$

Equations (26) and (27) describe the most general case, both for the non-local and local EEDFs. Analysis of both approaches can be found in the literature [115]. A non-local EEDF means that the electron velocity distribution at a given point is influenced by the electric field in other spatial regions. This happens when the mean free path of electrons is high compared to spatial gradients, which is typical for low pressure plasmas, especially in near-electrode regions. In most practical cases related to the relatively high pressure conditions of plasma-assisted combustion, it is possible

to restrict the consideration to the local case (also called "local field approximation", LFA).

The EEDF, $g(\epsilon)$, is related to the velocity distribution function $f(\mathbf{v})$ as follows:

$$g(\epsilon)d\epsilon = 4\pi v^2 f(\mathbf{v})dv, \tag{28}$$

where ϵ is the electron energy. In various books, the reader may encounter different notations for the electron energy distribution function, including $n(\epsilon)$, $g(\epsilon)$, or simply $f(\epsilon)$. However, for clarity in this section, we will adopt the notation from [90] and use $g(\epsilon)$ for the EEDF to avoid any potential misinterpretation. Using the relation between ϵ and v, it is possible to write for the EEDF

$$g(\epsilon) = 2\pi \left(\frac{2e}{m_e}\right)^{3/2} \sqrt{\epsilon} f(v(\epsilon)) = \rho(\epsilon) f(v(\epsilon)) \sim \sqrt{\epsilon} f(v(\epsilon)), \tag{29}$$

where ϵ is in eV and $\rho(\epsilon) \sim \sqrt{\epsilon}$ is the density of electron states along the energy axis. The electron density n_e is then determined as

$$n_e = \int_0^\infty g(\epsilon)d\epsilon, \tag{30}$$

and the average electron energy $\langle\epsilon\rangle$ as:

$$\langle\epsilon\rangle = \frac{1}{n_e}\int_0^\infty \epsilon g(\epsilon)d\epsilon = \frac{3}{2}\, T_e, \tag{31}$$

where T_e is the electron temperature in eV.

We now come back to the Boltzmann equation (26). Two analytical expressions for the electron distribution can be obtained for the specific case of purely elastic losses. Assuming constant collision frequency between electrons and neutral species ($\nu_{en} = const$), the Maxwellian distribution is obtained:

$$f_{Maxwell} \sim \exp(-\epsilon/T_e), \tag{32}$$

The mean electron energy for the Maxwellian distribution is equal to

$$T_e(Maxwell) = \frac{e^2E^2M}{3m^2(\nu_{en})^2} \sim \left(\frac{E}{N}\right)^2. \tag{33}$$

If the assumption is now changed to a constant mean free path length for the electrons, the solution of the Boltzmann equation is the Druyvesteyn distribution, given by:

$$f_{Druyvesteyn} \sim \exp(-\epsilon^2/(eE\lambda_e)^2), \tag{34}$$

where λ_e represents the mean free path length of electrons. The Druyvesteyn distribution decreases with energy much faster than the Maxwellian distribution for the same mean energy. For the Druyvesteyn distribution, the mean electron energy, and so the electron temperature, is proportional to the reduced electric field:

$$T_e(Druyvesteyn) \sim \left(\frac{E}{N}\right). \tag{35}$$

A detailed comparison of the two functions can be found in [85, 89]. The more general situation of a low temperature nonequilibrium plasma with inelastic losses cannot be described within the model cases $\nu_{en} = const$ or $\lambda_e = const$. No simple analytical solution exists for the mean electron energy/electron temperature in this case, but the electron temperature is always a monotonically increasing function of the reduced electric field. The function depends upon the gas mixture composition, the cross-sections of electron impact, the ionization degree, and so on. Note that the term "effective electron temperature" is usually used if the distribution function is not Maxwellian.

Solving the Boltzmann equation for the EEDF generally requires the use of numerical methods. In most studies, a solution is sought in the form of an expansion in spherical harmonics, considering the first two terms of the expansion. This is known as the two-term approximation of the Boltzmann equation, given by:

$$f(\mathbf{v}, t) = f^{(0)}(v, t) + f^{(1)}(v, t)\cos\Theta, \tag{36}$$

where $f^{(0)}$ is the isotropic part of the solution, $f^{(1)}$ the anisotropic part and Θ the angle between the directions of the electron velocity vector $\vec{v}$ and the electric field vector $\vec{E}$. Electrons acquire energy from the electric field applied to the plasma. Transferring this energy to atoms and molecules of the medium, which occurs most frequently in elastic collisions, is hindered by the relatively small mass of the electron. The energy fraction transferred during these collisions is $\delta_{em} = m_e/M$ where m_e is the electron mass and M is the mass of the heavy particle participating in the collision. The cross-sections of inelastic processes are generally smaller than elastic scattering, but the electron may transfer a significant portion of its energy.

Although the fraction of energy transferred to an electron in collisions with heavy particles δ_{em} is small, and the energy transfer in electron-electron collisions is very efficient, $\delta_{ee} \sim 1$, the effective (*i.e.*, multiplied by the energy transfer fraction) frequency of electron-electron collisions in weakly ionized plasma is generally much lower than the effective frequency of electron collisions with heavy particles:

$$\nu_{ee}\delta_{ee} << \nu_{em}\delta_{em}. \quad (37)$$

As a result, in weakly ionized nonequilibrium plasmas, the electron energy distribution function exhibits significant deviations from equilibrium, with the mean electron energy substantially exceeding that of the heavy particles. In contrast, in highly ionized plasmas, the EEDF tends to relax toward a Maxwellian distribution (see [116] for a detailed discussion of the conditions and parameters governing this transition).

The ratio of the anisotropic component $f^{(1)}$ of the EEDF to the isotropic component $f^{(0)}$ is on the order of the ratio of the drift velocity v_{dr} to the mean electron velocity. In weakly ionized plasmas with a relatively low electric field, the drift velocity is much smaller than the mean electron velocity [85], therefore the influence of $f^{(1)}$ can be neglected. The electron distribution function is close to Maxwellian in either very weak electric fields (where the main energy exchange occurs in elastic collisions with extremely low efficiency), or at high electron densities (where electron-electron collisions efficiently bring the distribution to a Maxwellian state, even in the presence of inelastic collisions).

Figure 9 presents a few examples of EEDFs calculated for different conditions. The dimension [$eV^{-3/2}$] is explained by a typical representation for the distribution function: the curve for the EEDF on the graph is actually $g(\epsilon)/(n_e\sqrt{\epsilon})$, see formulas (26)-(29). The figure illustrates two important effects related to EEDF and plasma chemistry. First, the electron energy distribution is a strong function of the reduced electric field, E/N. At 50 Td, the EEDF strongly decays between 10 and 20 eV. At 200 Td, the strong decay corresponds to higher energies, 20-30 eV. Comparing with the ionization thresholds (see Table (1)), it is possible to say that for 200 Td, the EEDF will provide efficient excitation of electronic states of atoms and molecules. Second, inelastic processes influence the shape of the EEDF significantly. Depending on the gas mixture composition, the EEDF can be different. Taking a stoichiometric H_2:O_2=2:1 mixture as a basis (solid orange and blue lines in Figure 9), we calculated the EEDF for the H_2:O_2=2:1 mixture diluted in 50% argon (dash lines), and for the same combustible mixture but this time diluted in 50% molecular nitrogen (dash dot lines). The presence of an atomic diluent such as argon evidently increases the population of the EEDF "tail" or, equivalently, increases the mean electron energy. This is due to the smaller number of internal degrees of freedom in an atomic gas compared to a molecular gas. The opposite effect is quite evident when observing the EEDF for the case of molecular nitrogen dilution: around 4 eV, the EEDF at E/N = 50 Td "dips". This dip is associated with the energy lost to excitation of the nitrogen molecule vibrational states. Both effects are much more pronounced for

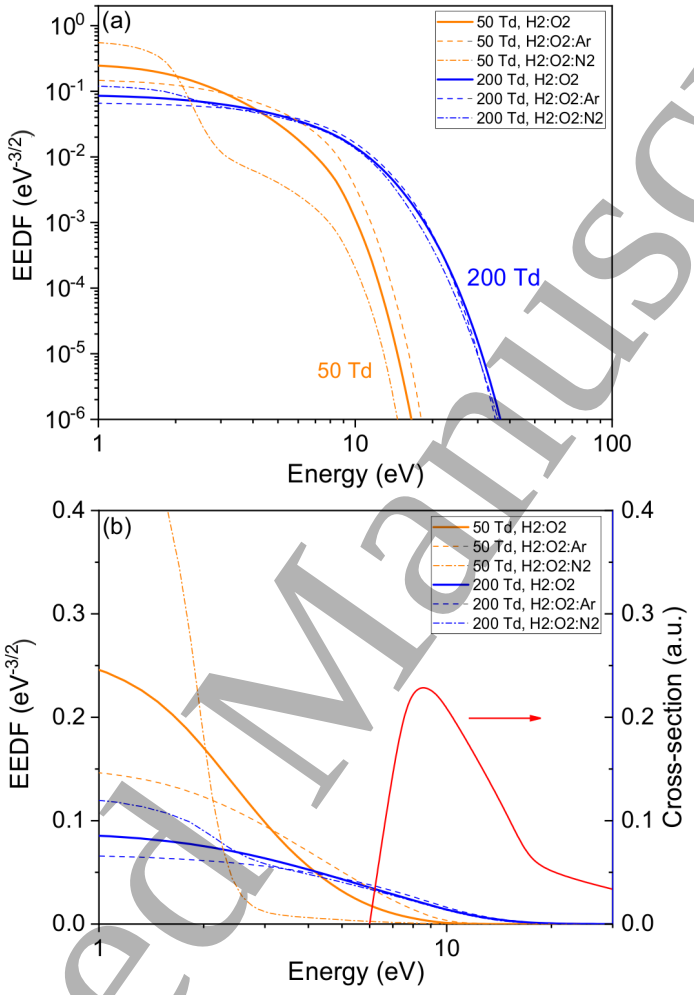

Figure 9: Electron Energy Distribution Function (EEDF) at different reduced electric field, E/N = 50 Td and E/N = 200 Td. Solid lines — EEDF in the H_2:O_2=0.668:0.332 mixture; dash line — EEDF in the H_2:O_2:Ar=0.334:0.166:0.5 mixture, and dash dot line — EEDF in the H_2:O_2:N_2=0.334:0.166:0.5 mixture: (a) in double logarithmic scale; (b) in semi-logarithmic scale. Cross-section of O_2 dissociation via electronically excited state with 6.1 eV threshold is shown in arbitrary units in red on the plot.

E/N=50 Td.

Thus, in chemically active mixtures, the E/N values and the gas composition related to chemical kinetics influence the EEDF and must be taken into account. Figure 9 also provides, as an example, a cross-section of O_2 dissociation via electronically excited state with 6.1 eV threshold. It is clearly seen that the "tail" of the EEDF and the rising, near-threshold, part of the cross-section, correspond to the same electron energies. The focus will now be on how to determine the rate constants of electron-impact processes using the EEDF and the cross-sections of electron collisions with atoms and molecules.

3.2.2 Cross-sections of electron collisions with atoms and molecules, rates of electron-impact processes, and energy branching

There is a fundamental difference in the approach to treating the kinetics of a combustion mixture in thermal equilibrium and the kinetics of a nonequilibrium plasma. In the former, the excitation of internal degrees of freedom of reactants is seen as a somewhat "exotic" phenomenon requiring separate consideration. In the latter, however, this is seen as a common occurrence, treated in all situations. Indeed, the typical adiabatic flame temperatures (the temperature of the products, after the chemical reaction, neglecting heat losses to the surroundings) for stoichiometric H_2:air and CH_4:air mixtures at atmospheric pressure are 2380 K and 2222 K respectively. For comparison, the average electron energy in a weakly ionized plasma is on the order of a few electronvolts, corresponding to a few tens of thousand of kelvins whereas the gas temperature can be much lower.

The rates of ionization, internal (rotational, vibrational, electronic) excitation and dissociation of gas molecules essential for plasma chemistry, are determined by collisions with electrons. To characterize a collision, it is necessary to know its corresponding cross-section. Cross-sections can be measured or obtained *via* quantum mechanical calculations. A cross-section of excitation/ionization is a function of electron energy. To "activate" a process, the electron energy must be higher than a given value called "the energy threshold". The ionization energies given in Table 1 are actually ionization thresholds ϵ_{th}^{ion}, the minimum energy for stripping an electron from an atom or molecule. The hierarchy of thresholds for inelastic collisions of electrons with molecules can be written as:

$$\epsilon_{th}^{rot} \sim (10^{-3}{-}10^{-2})\, eV < \epsilon_{th}^{vib} \sim (0.1{-}1)\, eV < \epsilon_{th}^{el} \sim (3{-}10)\, eV < \epsilon_{th}^{ion} \sim 10\, eV \quad (38)$$

where ϵ_{th}^{i} is the threshold energy of the i^{th} process and indexes "ion", "el", "vib"

and "rot" stand for ionization and excitation of electronic, vibrational and rotational levels, respectively.

Detailed information about excitation of different degrees of freedom of atoms and molecules can be found in the literature, specifically tutorials [117, 118] and books [119] describing the principles of plasma spectroscopy. The authors recommend reading such references for more information on how excitation by electron impact and the resulting transitions in atoms and molecules can be analyzed using the fundamentals of quantum mechanics. This will not be discussed further as it falls outside the scope of this article.

Ionization or excitation of molecules by electron impact is generally described by reactions of the form:

$$e + \mathrm{M} \rightarrow 2e + \mathrm{M}^{+}; \tag{39}$$

$$e + \mathrm{M} \rightarrow e + \mathrm{M}^{*}. \tag{40}$$

Unlike in equilibrium combustion chemistry, accounting for reverse processes is not always necessary in this case. At low degrees of ionization, that is, 10^{-3} to 10^{-4} and below, the probability of the reverse reactions (39), (40) is negligible.

The rate of excitation (40) of internal degrees of freedom (rotational, vibrational, or electronic excitation) is written as

$$\frac{d[\mathrm{M}^{*}]}{dt} = k n_e [\mathrm{M}], \tag{41}$$

where the rate constant k is defined as

$$k = \langle \sigma v \rangle = \sqrt{\frac{2e}{m_e}} \int_{\epsilon_{th}}^{\infty} \sigma(\epsilon) \epsilon f(\epsilon) d\epsilon, \tag{42}$$

and where $\sigma(\epsilon)$ is a cross-section of excitation and ϵ_{th} is a threshold energy.

The rate of excitation of internal degrees of freedom depends significantly on the electron energy ϵ. Two parameters should be considered: the threshold energy ϵ_{th} and the cross-section $\sigma(\epsilon)$. Excitation of a certain level, dissociation, or ionization, is impossible until at least some electrons acquire energy above the threshold value of a particular process:

$$\epsilon \geq \epsilon_{th}. \tag{43}$$

Due to the large difference in excitation thresholds of individual levels by electron impact, comparing the emission intensity of two optical transitions corresponding

to molecular bands with significantly different excitation energies/cross-sections can serve as a measure of electron energy (or reduced electric field E/N) [120–122]. The most commonly used optical transitions are the second positive system (SPS) of molecular nitrogen, $N_2(C^3\Pi_u) \rightarrow N_2(B^3\Pi_g)$, and the first negative system (FNS), $N_2^+(B^2\Sigma_u^+) \rightarrow N_2^+(X^2\Sigma_g^+)$. The thresholds of direct excitation by electron impact of the higher states $N_2(C^3\Pi_u)$ and $N_2^+(B^2\Sigma_u^+)$ are equal to 11.03 eV and 18.6 eV, respectively. As an illustration of the dependence of the rates of electron-impact processes on the reduced electric field, figure 10a shows the rate constants of excitation of $N_2(C^3\Pi_u)$ and the ionization of N_2 by electron impact, with thresholds of 11.03 eV and 15.6 eV, respectively.

Knowledge of the rate constants of individual processes in a gas mixture allows one to calculate the proportion of each process in the overall energy balance. Much like the rate constants, this proportion is a function of the reduced electric field. The energy share of all the different processes as a function of the reduced electric field is known as the energy loss fractions or the energy branching [13, 114].

An example of this energy branching calculated for H_2:O_2:Ar=2:1.2 mixture [123] is shown in Figure 10b. At low electric fields, 10−20 Td, about 55% of the energy goes into the vibrational excitation of H_2. This energy either participates in the chemical reactions, or is released as heat on characteristic timescales of VT-relaxation, τ_{VT}. This range of reduced electric fields is typical for the positive column of a glow discharge [85]. This channel decreases significantly with E/N, down to only 5% at 100 Td. In the same field range, about 10 Td, effective excitation of low electronic states can occur, for example $O_2(a^1\Delta_g)$, $\epsilon_{th} = 1.2$ eV. This long-lived state can significantly affect the kinetics of chemical reactions [16, 124]. However, it is less efficient compared to oxygen atoms produced by dissociation by electron impact [125, 126]. Dissociation of O_2 and H_2 via electronically excited states is designated as "diss O_2" and "diss H_2", respectively. It is seen that the corresponding fractions of energy loss increase with increasing E/N up to a maximum at approximately 100 Td. This is common for different mixtures. For example, in C_nH_{2n+2}:O_2:Ar, $n = 1 - 5$ mixtures, up to 80% of the energy goes into oxygen dissociation [127, 128] for the considered range of electric fields. The ionization of atoms and molecules becomes dominant at $E/N > 500$ Td.

It should be noted that plasma does not possess exceptional selectivity in the excitation of internal states of atoms and molecules the way that laser radiation does. However, in practical applications, the choice of the reduced electric field can ensure dominant excitation of certain states, which is well illustrated in Figure 10b. The high electric fields are, however, incompatible with high electron density: as the electron density increases, the electric field decreases. Typically, in the range of

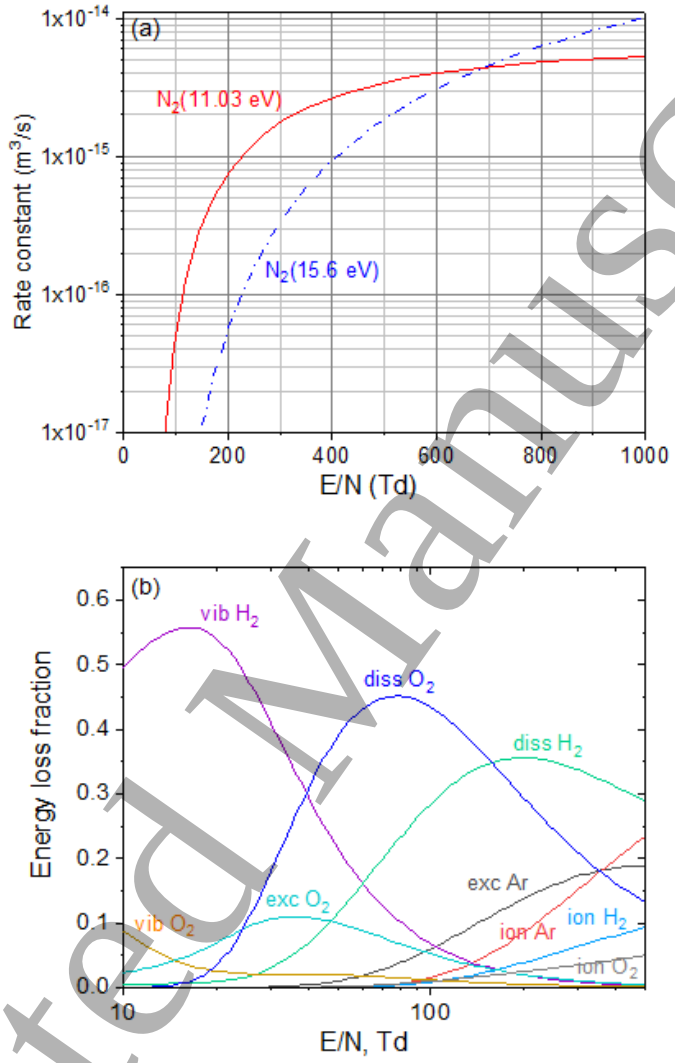

Figure 10: Reduced electric field E/N governing processes in plasmas: (a) rate constants of excitation of $N_2(C^3\Pi_u)$ (threshold 11.03 eV) and ionization of N_2 (threshold 15.6 eV); (b) energy branching (fraction of energy spent for a given process) calculated for H_2:O_2:Ar=2:1:2 mixture [123].

hundreds of Td, one will find thin electrode layers (*e.g.* the cathode and anode layers of a glow discharge) and discharges where the gas residence time in the discharge region is limited due to the geometry (*e.g.* dielectric barrier discharges (DBDs) when each microdischarge lasting tens of nanoseconds closes onto a new region of the dielectric surface) or due to conditions such as rapid gas flow through the plasma zone. Transient plasmas of nanosecond discharges are characterized by high electric fields and at the same time high electron densities, and so, are excellent candidates for efficient dissociation.

3.2.3 Dissociation of molecules by electron impact in plasma

Electron impact is able to stimulate dissociation of molecules by both vibrational and electronic excitation. Vibrational excitation happens to a few lower vibrational levels; then the dissociation proceeds via a non-direct multi-step process of V-V (vibrational-vibrational) exchange allowing molecules "to climb" a ladder of vibrational levels up to the dissociation threshold. This process is shown to be effective for some molecules, in particular for CO_2 [129, 130]. More theoretical information on this subject can be found in [89].

Dissociation through electronic excitation can proceed in just one collision but needs higher electron energies and so higher E/N values in the discharge. Different scenarios of dissociation [89] are schematically presented in Figure 11 and described below:

- Mechanism A is a direct excitation of a molecule from the ground state to a repulsive state followed by dissociation. As far as the electron energy significantly (few electron volts) exceeds the dissociation threshold, the reaction products can be high-energy neutral fragments ("hot atoms"). These hot atoms quickly increase the gas temperature *via* thermalizing collisions.

- Mechanism B is a direct excitation of a molecule from the ground state to an attractive state of energy higher than the dissociation threshold ϵ_D, resulting in dissociation. The products are non-excited fragments.

- Mechanism C is a direct excitation of a molecule from the ground state followed by radiative transition to a low-energy repulsive state and dissociation. The energy of the dissociation fragments in this case is similar to those of mechanism A.

- Mechanism D starts similar to mechanism C but is followed by radiationless transfer to a highly excited repulsive state and dissociation. This mechanism

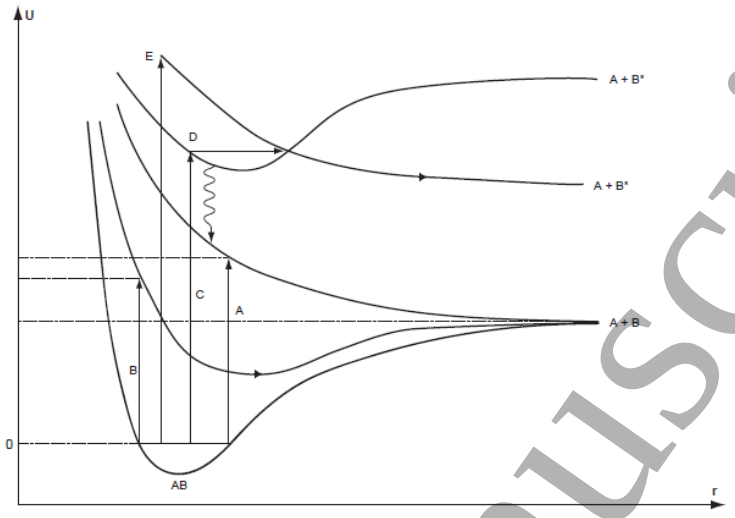

Figure 11: Mechanisms of dissociation through excitation by electron impact [89].

is usually referred to as predissociation.

- Mechanism E is similar to mechanism A and consists of direct electronic excitation from the ground state to a repulsive state with the difference that the repulsive state is higher in energy and the products are electronically excited fragments of the initial molecule.

The characteristic time of electron collisions with molecules is short, $\tau_e \sim 10^{-16}$ s. It can be estimated by dividing the molecule's size by the electron's velocity. This time τ_e is much shorter than the lifetime of molecules in either stable or unstable excited states. Consequently, dissociation by a single electron collision should be viewed as a two-step process: excitation, by electron impact, of a transition state and its subsequent decay.

It is interesting that the world's first experimental study of a transitional complex of a chemical reaction was precisely in the case of a dissociation. This experiment investigated the photo-dissociation process of the ICN molecule under the action of femtosecond laser radiation [131]. It resulted in Zewail being awarded the Nobel Prize in Chemistry in 1999 "for his studies of the transition states of chemical reactions using femtosecond spectroscopy." The CN buildup time measured in this already classical experiment [131] was reported to be 600 ± 100 fs.

In nanosecond discharges in air and N_2:O_2 mixtures [125, 132–134] at high electric fields, the maximum oxygen dissociation rate is achieved through dissociation

by direct electron impact. However, in the early afterglow, dissociative quenching reactions of excited nitrogen molecules by O_2 become the dominant process [135]:

$$N_2(A^3\Sigma_u^+, B^3\Pi_g, a'^1\Sigma_u^-, C^3\Pi_u) + O_2 \rightarrow N_2 + O(^3P) + O(^3P, ^1D) \quad (44)$$

The combined efficiency of these two processes enables fast, (tens of nanoseconds) [132] and significant (up to 100%) oxygen dissociation in nanosecond discharges [132, 134].

The Soviet school of plasma chemistry has provided detailed already classic reviews on dissociation in nonequilibrium plasma [113,136,137]. It is the sincere belief of one of the authors of this article that the ideas presented in these texts (only partially translated [136] at the time of writing) hold great importance for the community and should be made available in English to the global community of scientists. The reviews by Slovetsky [113,137] consider both existing methods for measuring dissociation cross-sections of molecules in plasma and a detailed quantum-mechanical approach to their calculation. Below, the mechanisms of dissociation of oxygen, hydrogen and methane by electron impact in gas discharges are discussed, according to [136, 137] and corresponding cross-sections are provided.

It is important to draw on related areas of plasma physics, as they can provide valuable insights and methods for the study of low-temperature plasmas. In this context, the website of the neutral gas transport Monte Carlo code EIRENE [138, 139], developed since the 1980s to investigate neutral gas transport in magnetically confined plasmas (currently including ITER), contains numerous detailed articles and reports spanning the period from 1994 to the present. In particular, these reports provide thorough quantum-mechanical analyses of ionization and dissociation processes in hydrogen and hydrocarbons, as well as generalized analytical formulas for the rates of these reactions (see, for example, [140]).

3.2.3.1 Dissociation of molecular oxygen

Electrons colliding with unexcited oxygen molecules can lead to dissociation due to transition to the repulsive branches of the potential curves of all states, converging to the first and second dissociation thresholds – 5.1 and 7.08 eV – $O_2(C^1\Sigma_u)$, $O_2(A^3\Sigma_u^+)$, $O_2(^3\Pi_g)$, $O_2(^3\Pi_u)$, $O_2(^1\Pi_g)$, $O_2(^5\Pi_g)$, $O_2(^5\Pi_u)$, and $O_2(B^3\Sigma_u^-)$. The cross-section of dissociation of $O_2(X^3\Sigma_g^-,\ v = 0)$ by electron impact through electronically excited states is presented in Figure 12.

Near the dissociation threshold, a significant contribution comes from the excitation of forbidden $O_2(A^3\Sigma_u^+)$ state with a threshold defined as the energy difference between the ground-state minimum and the vertical intersection with the upper

potential curve, around 6 eV. The main contribution to the total dissociation cross-section of oxygen through excitation of the electronic-vibrational levels by electron impact is *via* the excitation to the $O_2(B^3\Sigma_u^-)$ state at about 8 eV. Autoionization states (states with excitation energy greater than the ionization energy) provide significant, up to 50%, input at electron energies higher than 30 eV.

The forbidden molecular transition $O_2(X^3\Sigma_g^-) \rightarrow O_2(A^3\Sigma_u^+)$ corresponds to very weak absorption bands in the region 250-300 nm, so-called Herzberg I band. Transition $O_2(X^3\Sigma_g^-) \rightarrow O_2(B^3\Sigma_u^-)$ is an allowed Schumann–Runge system, well-known in plasma physics and combustion. This molecular transition is responsible for a strong temperature-dependent molecular bands absorption in 175-200 nm which transforms to continuum below 175 nm, and is responsible for existence of the vacuum ultraviolet (VUV) region in atmosphere of our planet [141].

3.2.3.2 Dissociation of molecular hydrogen

The lowest excited triplet state of molecular hydrogen $H_2(b^3\Sigma_u^+)$ is unstable. Excitation of this level, as well as $H_2(a^3\Sigma_g^+)$ and $H_2(c^3\Pi_u)$, from which cascade transitions to $H_2(b^3\Sigma_u^+)$ are observed, lead to dissociation. Additionally, transitions to repulsive branches of the potential curves of the $H_2(B^1\Sigma_u^+)$, $H_2(C^1\Pi_u)$ and $H_2(B'^1\Sigma_u^+)$ states result in dissociation with the appearance of excited atoms. Transitions to $H_2(D^1\Pi_u)$ with subsequent spontaneous predissociation, as well as decay from a number of Rydberg states, including autoionization states, also lead to dissociation with production of excited atoms.

The dissociation of hydrogen therefore varies with the electron energy (see Figure 13): at low electron energies, it occurs *via* excitation of the triplet states; and at energies above 50 eV, dissociation *via* higher electronic states with formation of excited atoms becomes the dominant mechanism.

3.2.3.3 Dissociation of methane

The total dissociation cross-section of methane, reconstructed from the data of [143] in the reviews [136, 137], is shown in Figure 14. Subtracting from this curve the dissociative ionization cross-section yields the cross-section of CH_4 dissociation through electronically excited states. This curve, in turn, represents the sum of the dissociation cross-section through excitation of allowed transitions and the dissociation cross-section resulting from excitation of forbidden transitions. In effect, any excitation of electronic levels of CH_4 that does not lead to ionization, results in dissociation. In this case, near the excitation threshold, the contribution of partial dissociation cross-sections through excitation of forbidden optical transitions becomes significant.

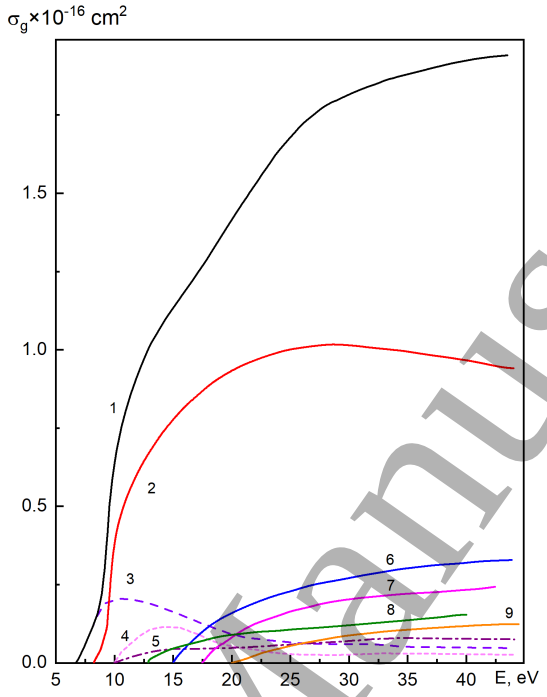

Figure 12: Cross-section of dissociation of $O_2(X^3\Sigma_g^-,\ v\ =\ 0)$ by electron impact through excited electronic states, recreated from [136, 137]: 1 – total cross-section; 2 – via $B^3\Sigma_u^-$ state; 3 – $\Delta\epsilon = 6.1$ eV; 4 – $\Delta\epsilon = 10.29$ eV; 5 – $\Delta\epsilon = 9.9$ eV. Autoionization levels: 6 – $\Delta\epsilon = 15.3$ eV; 7 – $\Delta\epsilon = 16.8$ eV; 8 – $\Delta\epsilon = 12.9$ eV; 9 – $\Delta\epsilon = 19.7$ eV;

Similar conclusions were drawn in [137] for other saturated hydrocarbons, namely ethane and propane. Note that limited information published by the same author is available in English: for example, [144] is devoted to the analysis of the mechanisms of dissociation of hydrocarbons containing 1 to 6 C-atoms, by DC, high-frequency and microwave discharges.

3.2.4 Specific energy deposition and G-value

While it is an important variable, the reduced electric field is only one of multiple similarity parameters of a gas discharge. There may be situations where, for a given

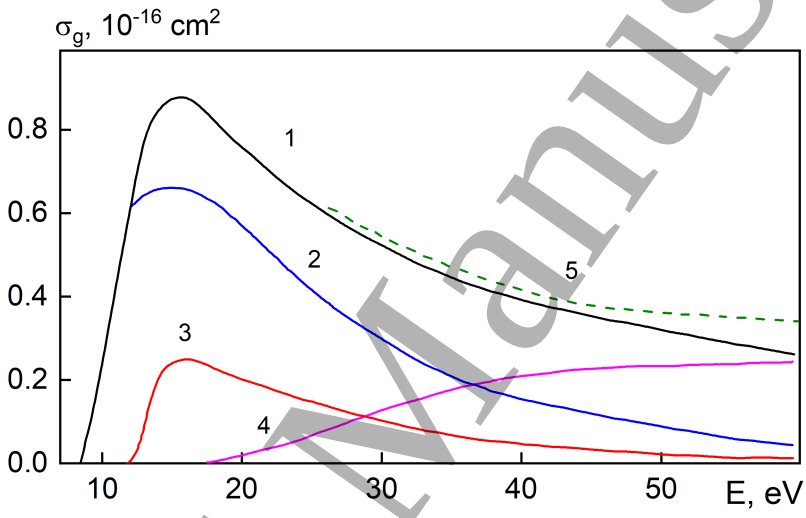

Figure 13: Total and partial dissociation cross-sections of $H_2(X^1\Sigma_g^+,\ v = 0)$ by electron impact through excited electronic states recreated from [136, 137]: 1 – total cross-section measured in [142]; 2 – via $b^3\Sigma_u^+$ state; 3 – via $a^3\Sigma_g^+$ state; 4 – with production of excited atoms $H(^2P)$ and $H(^2S)$, at least by 50% via $B'^1\Sigma_u^+$, $B^1\Sigma_u^+$, and $C^1\Pi_u$ states; 5 – sum of the partial cross-sections (2)-(4).

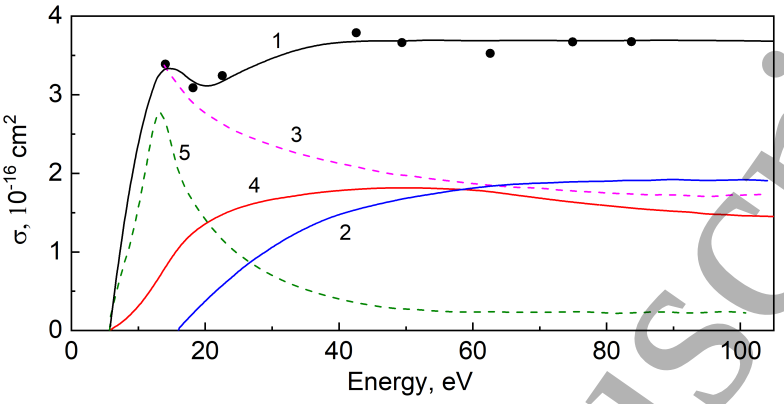

Figure 14: Total and partial dissociation cross-sections of CH_4 by electron impact recreated from [136, 137]): 1 – total cross-section of dissociation, symbols – data according to [143]; 2 – dissociative ionization cross-section; 3 – total dissociation cross-section through electronic-vibrational levels; 4 – through excitation of allowed transitions; 5 – through excitation of forbidden transitions.

field, the specific energy deposition in the plasma (SED, the energy divided by the number of particles) varies extensively. A simple example of this is the nanosecond fast ionization wave (FIW) discharge [133, 145]. For the same high-voltage pulse on the electrodes, the SED in the case of a 20 mm diameter discharge tube is around 10^{-3} eV/particle [145], but reducing the diameter to 2 mm leads to an increase to $\omega = 1 - 3$ eV/particle [133]. As a result, for a 30 ns high-voltage pulse, the electron density in spatially uniform homogeneous plasma can vary from $n_e = 10^{11} - 10^{12}$ cm^{-3} [145] to $n_e = 10^{15}$ cm^{-3} [133] in different set-ups.

Another important parameter is the G-factor (or G-value), defined as the energy (in eV/particle) required to form a given particle, or its reciprocal (in particles/eV). G-values are used to compare plasma-chemical processes in different discharges. Calculating the G-value is not simply a matter of taking the threshold energy or the individual cross-section of the considered process: the G-value takes into account the energy expenses for all processes according to different pathways for a given electric field and deposited energy. It can give, for example, the energy required to form an oxygen atom.

Note that a significant increase in the specific energy delivered to the system at high E/N values may alter the system kinetics [133]. While the plasma remains in nonequilibrium, the elevated electron density and enhanced collisions of excited species with neutrals, other excited particles, and electrons can significantly impact

the plasma chemistry.

3.2.5 Fast gas heating

Nonequilibrium low temperature plasmas are often considered a medium where reaction rates are independent of the gas temperature. This can be true in particular cases such as low SED weakly ionized plasmas, but in general this is not correct, especially in combustion applications or any other process sensitive to temperature. In this case, the heat released in collisional relaxation from excited/charged heavy particles in plasma and afterglow must be taken into account. Two mechanisms are identified, fast gas heating (FGH), mainly *via* excited electronic states of atoms and molecules, and vibrational-translational (VT) relaxation, the latter taking place several orders of magnitude slower than the former.

Fast gas heating can drastically impact the chemistry on a very short timeframe. For example, a discharge initiated by a high-voltage pulse of 6 kV in amplitude in a 4-mm gap at atmospheric pressure air preheated to 1500 K produces a temperature increase of about 900 K within 30 ns, corresponding to a fast heating rate of $5 \cdot 10^{10}$ Ks^{-1} [132]. Figure 16 reproduces synchronized measurements of voltage (re-calculated to E-field), current, temperature measured by optical emission spectroscopy (OES) from the transition of the 2^+ system of molecular nitrogen, $N_2(C^3\Pi_u)$ $\rightarrow N_2(B^3\Pi_g)$, and densities of excited species measured by absolute emission spectroscopy or cavity ring-down spectroscopy. Results of numerical calculations of gas temperature and O–atom density from [146] are presented by curves (1) and (2), respectively, in the same figure.

Note that in plasma-assisted combustion in the presence of N_2, the 2^+ system is the most often used transition to measure the temperature by OES. Unlike in combustion where the thermodynamic equilibrium conditions imply that emission from rotational lines provides direct information about the gas temperature, in plasma it is necessary to analyze whether the rotational temperature is equilibrated with the bulk temperature of the gas. The general principles of this analysis can be found in [152, 153]; an analysis related to nanosecond discharges can be found in [133]; and a model to infer the gas temperature from the measured rotational temperatures of excited N_2 species is presented in [153].

A recent review [21] analyzed energy transfer and fast gas heating in air together with the limited data in combustible mixtures. Figure 16 reproduces the fraction of total energy delivered to plasma spent on fast gas heating, η_R. The value of η_R is a function of the reduced electric field in the discharge and practically does not depend upon the electron density and gas pressure. Calculations [21]

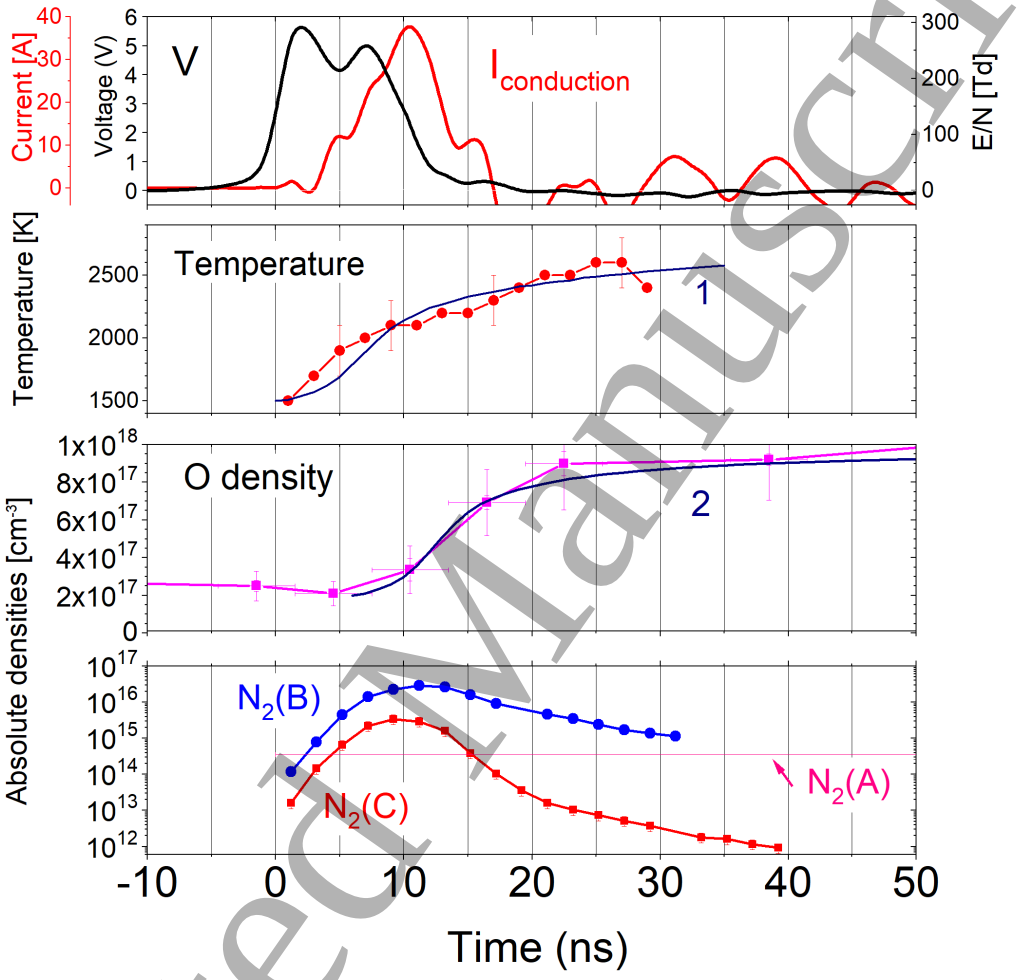

Figure 15: Synchronized measurements of discharge current, voltage, temperature, O-atoms density, $N_2(A^3\Sigma_u^+)$, $N_2(B^3\Pi_u)$, $N_2(C^3\Pi_u)$ densities in air excited by nanosecond repetitive pulsed (NRP) discharge with 0.67 mJ/pulse. The measurement of $N_2(A^3\Sigma_u^+)$ is an average value over 50 ns [132]. Curve (1) on the temperature plot and curve (2) on [O]–atoms plot are the results of numerical calculations adapted from [146].

are in good agreement with the experimental data [132, 147–151], possible overestimates of experimentally measured η_R at 200-1000 Td being discussed in [21]. It is seen that the energy fraction spent on FGH increases with E/N from about 10% at 100 Td to 30% at 200 Td. The energy efficiency of FGH calculated with the model of Popov [125, 154] is given by curve (I) in figure 16; the maximum theoretically possible value $\eta_R^{max}(E/N) = 100\% - \eta_{diss}(E/N)$ is given by curve (II). Here, η_{diss} is the fraction of the discharge energy spent to dissociate nitrogen and oxygen molecules, calculated using BOLSIG+ code [114] assuming that quenching of electronically excited states $N_2(A^3\Sigma_u^+$, $B^3\Pi_g$, $C^3\Pi_u$, $a'^1\Sigma_u)$ by molecular oxygen results in O_2 dissociation. The most important processes leading to fast gas heating are the following reactions [21, 135]: quenching of $N_2(C^3\Pi_u)$ by molecular oxygen; quenchiPashen's law, derived for a static breakdown voltage, separates the region between "no discharge" (below the curve) from the region of "Townsend discharge" (above the curve). The Townsend mechanism describes a glow discharge, when separate electron avalanches provide a uniform pattern. In the case of pulsed voltage, the situation changes. Streamer mechanism of breakdown dominates when the electric

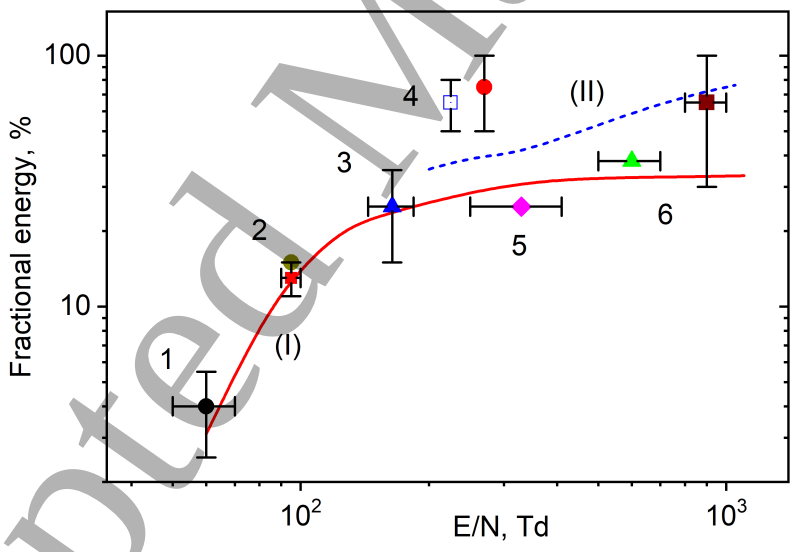

Figure 16: Fraction of energy spent on fast gas heating η_R (or the energy efficiency of FGH) as a function of E/N [21]. Symbols represent the experimental data: 1 - [147], 2 - [148], 3 - [132], 4 - [149], 5 - [150], 6 - [151]; lines are the results of calculations [21].

field in the head of a single avalanche becomes comparable to the external electric field. The modified Pachen's law should take into account an overvoltage (percent of voltage above a static breakdown threshold) as a function of *pd*. More details about triggering and development of pulsed discharges can be found elsewhere [105]. ng of $N_2(B^3\Pi_g)$ by molecular oxygen; reactions involving charged particles; dissociation of N_2 molecules by electron impact followed by quenching of $N(^2D)$ atoms; quenching of excited $O(^1D)$ atoms by N_2; dissociation of O_2 molecules by electron impact; quenching of excited $N_2(A^3\Sigma_u^+)$ and $N_2(a'^1\Sigma_u^-)$ molecules by O_2.

Theory and practical data for VT-relaxation are not discussed in this review and can be found in [155, 156].

3.2.6 Notions of different equilibria

Over the course of this review, several different types of equilibria are described. Both plasma and combustion physics will have their own definitions, this section therefore aims at presenting all major definitions in one place.

A plasma is said to be in thermal equilibrium (TE) when the temperature Th of heavy species, neutral and ions, is equal to the temperature of the free electrons, i.e. $T_h = T_e$. These temperatures are also called the translational temperatures because they are related to the kinetic energy of translational motion , not to the excitation of internal degrees of freedom. It is important to emphasize that plasmas in thermal equilibrium may feature nonequilibrium population distributions of electronic, vibrational and rotational levels, since those are controlled by chemical reactions that may not be equilibrated. Thus, in thermal equilibrium, one may have electronic, vibrational and rotational temperatures that differ from $T_h = T_e$.

Chemical equilibrium (CE) corresponds to the case where all chemical reactions are equilibrated, including those involving atomic or molecular species in excited internal energy levels (electronic, vibrational and rotational).

The plasma is in Local Thermodynamic Equilibrium (LTE) when the system is both in thermal and chemical equilibrium locally (i.e. in small volume elements): LTE = TE + CE. In Local Thermal Equilibrium, the plasma composition and the distribution over the internal energy levels can then be obtained directly from the local pressure and temperature. In LTE plasma, however, the radiative field is not necessarily in equilibrium, and as a result the plasma spectrum features discrete lines of atoms and molecules.

Finally, if the plasma is in thermal, chemical and radiative equilibrium (i.e. no net emission or absorption), the system is said to be in Complete Thermodynamic Equilibrium (CTE). The radiation emitted by the plasma is then of the blackbody

type. To imagine CTE plasma, [89] suggests that the plasma volume must be large, such that its central part is homogeneous and not sensitive to boundaries. In fact, CTE plasmas typically require large volumes and high pressures. They are usually not obtained in typical laboratory experiments, but rather in large system such as the core of the Sun.

n pure combustion applications, it is generally considered that the gas is in thermal equilibrium, which implies that chemical kinetics can be described by a single temperature. In gas discharges, however, the applied electric field accelerates the free electrons, resulting in electron temperature higher than the gas temperature. The relation between the electric field and the electron temperature is discussed in section 3.2.1. Thus the kinetics of gas discharges are generally described by a combination of rate constants depending either on the gas temperature or on the electric field.

3.3 On numerical modeling of plasma chemistry

Since the scope of this review is limited, we do not address self-consistent two-dimensional modeling of gas discharges that simultaneously solve transport equations for charged and neutral species, Poisson's equation for the electric potential, and the electron energy conservation equation, coupled with detailed plasma chemistry. The most extensive data are available for non-reactive gases; the reader is referred to the review [157], which discusses the physics of streamer discharges from both experimental and modeling perspectives. In modern plasma physics, 2D simulations of gas discharges in combustible mixtures with full plasma kinetics are actively being developed; for instance, an atmospheric-pressure streamer in a hydrogen–air mixture is modelled in [158]. Codes that have been developed and validated over decades within research groups often become internationally recognised and widely used in different groups over the world, such as nonPDPSIM [159,160]. Recently, openly accessible 2D parallel plasma solvers with detailed chemical kinetics have also emerged, see PASSKEy website [161,162]. This work's scope will however focus on 0D kinetics and on available plasma chemistry solvers.

3.3.1 Overview of kinetic solvers for nonequilibrium plasmas

Calculations of EEDF in molecular gases appeared in the literature in the 1960's and 1970's. A detailed analysis of Boltzmann equation solvers for the EEDF in stationary fields, calculation results and review of previous works on numerical determination of EEDF, as well as analysis of energy branching in atomic and molecular gases up to

1980 can be found in [112]. Since then, research groups have used various databases and original codes and approaches [163] to solve the Boltzmann equation.

One of the early codes, which became widely known and frequently cited, is GlobalKin [164, 165]. The code consists of three main modules: a reaction chemistry and transport module, a Boltzmann equation solver for the electron energy distribution (EED), and an ordinary differential equation (ODE) solver module. The Michigan Institute for Plasma Science and Engineering (MIPSE) website [166] provides links to numerous scientific studies in which calculations were performed using GlobalKin. The website also hosts a large collection of video seminars by experts, spanning from 2009 to 2025. These seminars constitute a valuable resource for the study and understanding of low-temperature plasma physics..

Over 20 years ago, scientists from LAPLACE (Laboratoire Plasma et Conversion d'Energie, Toulouse, France) initiated the development of a numerical code to solve the Boltzmann equation (26) to make it accessible to all specialists in the field of low temperature plasma physics [114]. BOLSIG+, the solver developed by that group [167], provides steady-state solutions of the Boltzmann equation for electrons in a uniform electric field using the classical two-term approximation, and has been used by a generation of scientists. The solver considers different growth models, quasi-stationary and oscillating fields, electron-neutral collisions, and electron-electron collisions. Currently, BOLSIG+ is the most commonly used freeware for solving the Boltzmann equation.

To use BOLSIG+, one needs the value of the electric field and a set of cross-sections. At least the cross-sections of elastic collisions are needed to calculate the EEDF: they define the shape of the electron energy distribution function in general. Cross-sections of inelastic collisions are responsible for the deformation of the EEDF in intervals of energy corresponding to different inelastic processes. It is the users' responsibility to validate their chosen sets of cross-sections. Cross-section sets in the database of BOLSIG+ are open-source and users should always verify if they are correct and complete, which should be done by correlation with data known in the literature. For example, for molecular nitrogen, a review of the electron-impact cross-sections can be found in classical papers [168, 169] or more recent papers containing calculations [170] and experiments [171]. Completeness is checked by swarm parameters, namely by comparing the calculation results with known experimentally measured drift velocity and the first Townsend coefficient. The users should also, especially at high electric fields, check how the cross-sections are extrapolated to the region of high electron energies.

The BOLSIG+ code calculates swarm parameters, EEDFs, reaction rates and energy branching (by dividing the energy loss coefficients by the sum of "elastic

power" and "inelastic power") as a function of the reduced electric field. The rates of electron-impact reactions thus obtained can be used for calculations of 0D kinetics or as a part of advanced self-consistent 2D numerical codes.

The role of LAPLACE scientists in the development of low temperature plasma over the last 30 years deserves to be emphasized: in 2010 the Gaseous Electronics Conference (GEC), a major international conference for the low temperature plasma science community, initiated the Plasma Data Exchange Project, PDEP [172]. The heart of the PDEP was the open-access website, LXCat [173, 174], developed by researchers at LAPLACE. LXCat is a platform for archiving and manipulating collections of data related to electron scattering and transport in cold, neutral gases, organized in databases provided by individual members or institutions of the low temperature plasma community.

They also developed ZDPlaskin [175], a free software to calculate plasma chemistry. This came about as a bit of a revolution, as the user-friendly interface provided easy access to modeling to the community, especially to experimentalists. It has now been more than 10 years that plasma experiments can be built in an iterative manner, with predictive modeling on the same time scale, providing better control and better experimental planning.

Both BOLSIG+ and ZDPlasKin are Fortran 90 codes. In ZDPlasKin, the list of species and reactions is provided by the user and re-formatted into a Fortran module that interfaces to an ordinary differential equation (ODE) solver. Reaction rates for electron collisions with atoms and molecules are calculated using BOLSIG+. Finally, the compiled code calculates the time evolution of species densities and reaction rates.

To continue the description of the set of tools available to calculate plasma chemistry, the open-source C++ code Pump-Kin (pathway reduction method for plasma kinetic models) [176], compatible with the output format of ZDPlasKin, was developed to reduce complex plasma kinetic mechanisms.

There are other free solvers of the Boltzmann equation. In particular, the LoKi-B [177–179] solver, developed recently by a group of scientists at IST-Lisbon, is an open-source simulation MATLAB tool solving a time and space independent form of the Boltzmann equation, for non-magnetized, nonequilibrium, low temperature plasmas excited by DC or RF electric fields. Similar to BOLSIG+, LoKI-B accepts input files with electron scattering cross-sections obtained from the LXCat open-access website [174].

Reference [179] compares, using the capabilities of the LoKI software, two cases: (i) a time-dependent formulation of the Boltzmann equation that considers an intrinsic time evolution for the EEDF; and (ii) a "standard" quasi-stationary approach, where the time-independent form of the Boltzmann equation is solved for different

reduced electric fields during the pulse. These cases are solved for different rise times of the electric field and for two pressures, 1 Torr and 1 bar. Significant differences were observed between non-stationary and stationary solutions at low pressures and fast (about nanosecond) changes of the electric field. The differences are most significant at the rising front of the pulse. Calculations [179] are performed for relatively low electric fields, not higher than 45 Td.

BOLtzmann equation solver Open Source library (BOLOS) [180] is another implementation based on the same algorithm as BOLSIG+ [114] but built in Python. It also accepts input files with electron scattering cross-sections obtained from the LXCat open-access website. The goal, described by the author, is to allow for simpler integration into other codes and automated pipelines, and to allow users across different operating systems to also benefit from the solver.

Already classical paper [181] provides a criterion of applicability of the stationary solution of the Boltzmann equation. A quasi-stationary description of the EEDF, swarm parameters and rate constants is valid when

$$\tau_\epsilon \nu_\epsilon >> 1, \quad \tau_\epsilon \sim \left(\frac{1}{E}\frac{\partial E}{\partial t}\right)^{-1}. \tag{45}$$

Parameter ν_ε, or frequency of energy relaxation, can be found by taking into account all collision processes for a given gas composition. This frequency, as a function of the electron temperature between 0.01 and 10 eV, can be found in [182] for H_2O, CO_2, C_3H_8, CH_4, CO, H_2 and O_2, and in [183] for N_2, O_2, air, CO_2 and Ar. From analysis of the equation (45) it follows [181] that, at atmospheric pressure, $T = 300$ K and $E/N \sim 100$ Td, the correction to the ionization rate constant in nitrogen does not exceed 0.25% – so can be considered as negligibly small. Note that a publication [184] of the LoKI group shows no difference in ionization in a pulsed nanosecond discharge in 10 Torr air with a maximum electric field of 300 Td, the ionization being calculated by time-dependent and stationary LoKI solvers. Recent paper [185] provides detailed comparative analysis between local-energy approximation (LEA), local-field approximation (LFA) and Monte-Carlo (MC) time-dependent calculations of processes in pulsed nanosecond plasmas. As far as plasma-assisted combustion is associated with relatively high gas pressures and electric fields, a quasi-stationary description of the EEDF can be used.

More information about the freeware solvers available in the field of low temperature plasma, including demonstration of their tests, can be found in the recent topical review "Foundation of plasma standards", section "Open source and publicly available codes" [186].

Looking at efforts made into merging the plasma and combustion tools, the au-

thors note that the sequential use, of BOLSIG+ for the electron energy distribution function (EEDF), a home-made ODE solver for plasma kinetics, and a combustion ODE solver such as CHEMKIN, which integrates chemical reaction mechanisms over time, was reported over 15 years ago [127] for CH_4-C_5H_{12} based mixtures. This work focused on linking electron-impact kinetics calculated with BOLSIG+ to the ChemKin-Pro solver and was published in 2015 [187]. This approach incorporated electron energy loss and inelastic collision rates into combustion reaction files for low temperature air, H_2–air, and hydrocarbon–air plasmas sustained by nanosecond pulse discharges. ChemKin-Pro is now a commercial software provided by ANSYS [188]. Over the past decade, the open-access code Cantera [189] has emerged as a widely used tool for solving the ordinary differential equations for combustion kinetics, with guidance and tutorials available [190]. A few representative examples from recent years show how plasma kinetics can be incorporated into combustion solvers based on Cantera. In [191], the effect of nanosecond discharge on the combustion characteristics of ammonia is investigated over a wide range of mixture properties and plasma settings. Reference [192] provides, for $CH_4/O_2/N_2$ mixtures, a zero-dimensional solver, tracking energy from the electrical input to thermal and chemical effects and identifying key plasma-activated pathways such as vibrational-translational relaxation, fast gas heating, and O_2 and fuel dissociation. Another recent paper [193], combining SENKIN code [194] and ZDPlaskin, study the ignition delay and NO emission characteristics of the $NH_3/N_2/O_2$ mixture under the influence of a nanosecond pulsed/DC hybrid plasma. Finally, ChemPlasKin [195], combines an electron Boltzmann solver with Cantera to compute time-resolved species concentrations and gas temperature in air, hydrogen-containing, and methane-containing mixtures under nanosecond pulse plasma, capturing both chemical kinetics and plasma-induced heating, including fast gas heating and slower vibrational–translational relaxation. More examples of modeling linking plasma and complex combustion systems can be found in the second part of this review [25].

3.3.2 On a practical side: why ready-to-use kinetic mechanisms are not available nowadays in the field of low temperature plasma science?

The difference between combustion kinetics and plasma kinetics is that in combustion, large, well-tested mechanisms were developed a few decades ago (see section 2.2.3 for details). These mechanisms use the gas temperature as the main parameter for Arrhenius rate constants. In some specific cases, rate constants can also depend on the pressure. In general, these mechanisms are quite universal and describe well-

defined, experimentally observed parameters, such as the ignition delay time. In plasma, no standard kinetic mechanisms exist, and each researcher must personally investigate the kinetic domain of interest. Large kinetic mechanisms and databases were created about 30 years ago for atmospheric physics (these data are compiled in [196]) and for gas laser physics. Reviews of reaction mechanisms for atmospheric gases can also be found [197] on the website of the International Union of Pure and Applied Chemistry (IUPAC), the web-resource on chemical nomenclature, terminology and standardized methods for measurement. Looking at the last decades, the most commonly used kinetic mechanism for air is the one of Kossyi *et al.* [198]. As underlined in Plasma Roadmaps 2017 review [5] by Pitchford and Turner, a kinetic mechanism is more than an assembly of rate constants. A mechanism is designed to predict certain species densities under specified conditions and will have been tested ('validated') by comparison with suitable experiments ('targets'). These aims will inform the selection of both the species and reactions represented in the mechanism, as well as the choice of target experiments. They also say that the low temperature plasma literature is replete with discussions of mechanisms for many different gas mixtures, but intercomparisons are generally difficult because of the disparity in the discharge conditions considered. At present, the low temperature plasma community lacks recommended mechanisms, developed and validated to the same level of detail as combustion mechanisms. Driven by the increasing cross-disciplinarity of plasma physics, the community should aim to invest into improved intercommunication. The goal should be to produce these comprehensive and accurate mechanisms, both to push the field forward but also to lower the barrier to entry into plasma physics for scientists and engineers of other fields.

4 Conclusion

To conclude, Part 1 of the Foundation paper "Plasma-Assisted Combustion: Tutorial Review" summarizes the available review articles and books on plasma-assisted combustion, covering the period from 2006 to the present. Over the past two decades, this field has evolved from the initial demonstrations of plasma-assisted ignition of combustible mixtures and gas flows in laboratory conditions to advanced real-time diagnostics, complex numerical modeling and experimental engine prototypes.

The tutorial presented in the first part offers readers fundamental insights into combustion and plasma physics, with a particular focus on low temperature plasma physics essential for understanding the field of plasma-assisted combustion. Given the limited format, the authors emphasize citations of original research papers and monographs to ensure that interested readers have access to the most relevant sources

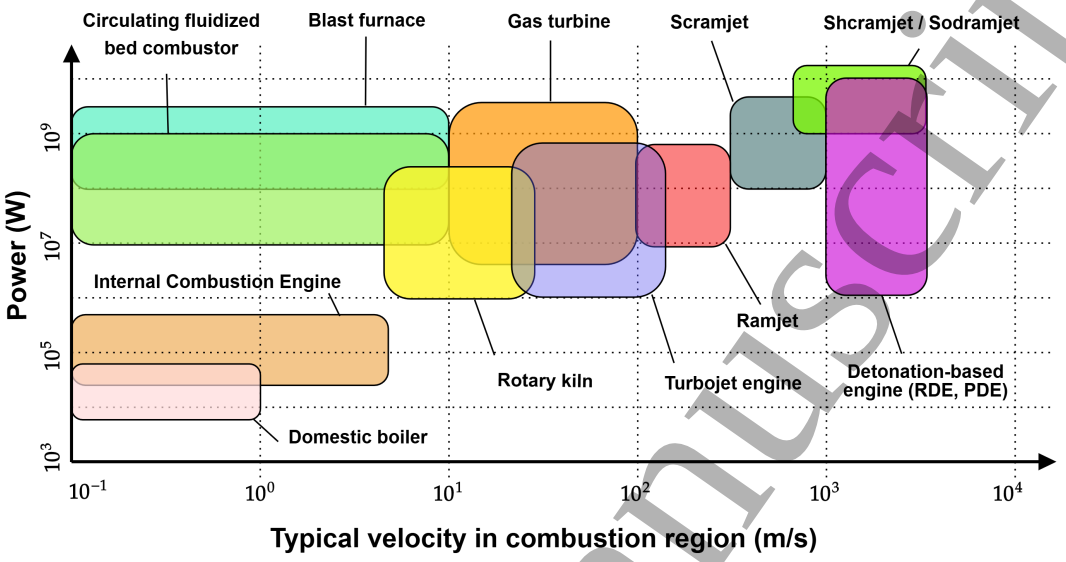

Figure 17: Typical powers and flow velocities in combustion applications. The orders of magnitude are indicative.

for further education in this area.

As a transition to the second part of this article, which discusses concrete applications of plasma-assisted combustion, figure 17 describes the different ranges of velocity in the combustion region and power for different processes. This illustrative plot, which should be interpreted with caution, serves as a visual aid to readers unfamiliar with real-life applications of combustion, and demonstrates the vast range of combustion speeds and power levels relevant to industrial and technical applications—spanning at least five to six orders of magnitude. Research in plasma-assisted combustion is ongoing in several of these fields to tackle issues relevant to each, demonstrating the versatility and wide domain of applicability of PAC. The diagram implicitly contains more parameters than just speed and power. In particular, the gas density plays a crucial role in determining the development of gas discharges and resulting plasma properties. It is important to note that the energy release in combustion reactions is extremely high, which is why combustion remains the primary energy source on Earth. The role of plasma is not to replace combustion but to modify ignition or combustion in a controlled manner, influencing this highly energetic process with a minimal part of its energy—less than a fraction of a percent. These

and other critical aspects are discussed in the second part of this foundation paper, which focuses on progress in mechanisms and applications of PAC [25].

Acknowledgments

The work of J.-B. P.-T. and C.O.L was partially supported by the European Research Council (ERC) under the GreenBlue project of the European Union's Horizon 2020 research and innovation programme (grant agreement No. 101021538). The work of S.M.S. was partially supported by the European Union project CAIPIRINH3A under grant agreement No. 101191768. The work of V.L. and S.M.S. was also partially supported by Agence de l'Innovation de Défense – AID - via Centre Interdisciplinaire d'Etudes pour la Défense et la Sécurité – CIEDS - (project 2022 - PPRINCE) and Energy4Climate Interdisciplinary Center (E4C) of IP Paris and Ecole des Ponts - ParisTech in the framework of the 3rd Programme d'Investissements d'Avenir, ANR-18-EUR-0006-02. Views and opinions expressed are however those of the authors only and do not necessarily reflect those of the European Union or CINEA. Neither the European Union nor the granting authority can be held responsible for them and for any use that may be made of the information contained in this article. For open access purposes, a CC-BY license has been applied by the authors to this document and will be applied to any subsequent version up to the author's manuscript accepted for publication resulting from this submission. The authors would like to thank Dr. Pierre Vidal, Dr. Alexander Konnov, Dr. Nikolay Aleksandrov, Dr. Nikolay Popov, Dr. Alejandro Alvarez, Dr. Daniel Durox, Dr. Sébastien Ducruix and Nicolas Vaysse for numerous discussions, valuable critiques, insightful proofreading, and constructive advice. The authors express their sincere gratitude to their colleagues and students for the privilege of working with them and for the inspiration they have provided over years and decades of research.

5 References

References

[1] Darecki M, Edelstenne C, Enders T, Fernandez E, Hartman P, Herteman J P, Kerkloh M, King I, Ky P, Mathieu M, Orsi G, Schotman G, Smith C and Wörner J D 2011 *Flightpath 2050. Europe's Vision for Aviation: Maintaining Global Leadership and Serving Society's Needs.* (Publications Office of the European Union) ISBN 978-92-79-19724-6

[2] IEA www.iea.org/reports/greenhouse-gas-emissions-from-energyoverview

[3] Law L C, Foscoli B, Mastorakos E and Evans S 2021 A Comparison of Alternative Fuels for Shipping in Terms of Lifecycle Energy and Cost *Energies* **14** 8502

[4] Samukawa S, Hori M, Rauf Sh, Tachibana K, Bruggeman P, Kroesen G, Whitehead J Ch, Murphy A B, Gutsol A F, Starikovskaia S, Kortshagen U, Boeuf J P, Sommerer T J, Kushner M J, Czarnetzki U and Mason N 2012 The 2012 Plasma Roadmap *J. Phys. D: Appl. Phys.* **45** 253001

[5] Adamovich I, Baalrud S D, Bogaerts A, Bruggeman P J, Cappelli M, Colombo V, Czarnetzki U, Ebert U, Eden J G, Favia P, Graves D B, Hamaguchi S, Hieftje G, Hori M, Kaganovich I D, Kortshagen U, Kushner M J, Mason N J, Mazouffre S, Mededovic Thagard S, Metelmann H R, Mizuno A, Moreau E, Murphy A B, Niemira B A, Oehrlein G S, Petrovic Z Lj, Pitchford L C, Pu Y K, Rauf S, Sakai O, Samukawa S, Starikovskaia S, Tennyson J, Terashima K, Turner M M, van de Sanden M C M and Vardelle A 2017 The 2017 Plasma Roadmap: Low Temperature Plasma Science and Technology *J. Phys. D: Appl. Phys.* **50** 323001

[6] Adamovich I, Agarwal S, Ahedo E, Alves L L, Baalrud S, Babaeva N, Bogaerts A, Bourdon A, Bruggeman P J, Canal C, Choi E H, Coulombe S, Donkó Z, Graves D B, Hamaguchi S, Hegemann D, Hori M, Kim H H, Kroesen G M W, Kushner M J, Laricchiuta A, Li X, Magin T E, Mededovic Thagard S, Miller V, Murphy A B, Oehrlein G S, Puac N, Sankaran R M, Samukawa S, Shiratani M, Šimek M, Tarasenko N, Terashima K, Thomas Jr E, Trieschmann J, Tsikata S, Turner M M, van der Walt I J, van de Sanden M C M and von Woedtke T 2022 The 2022 Plasma Roadmap: Low Temperature Plasma Science and Technology *J. Phys. D: Appl. Phys.* **55** 373001

[7] Starikovskaia S M 2006 Plasma Assisted Ignition and Combustion *J. Phys. D: Appl. Phys.* **39** R265–R299

[8] Matveev I B and Rosocha L A 2006 Special Issue on Plasma-Assisted Combustion *IEEE Transactions on Plasma Science* **34** 2469–2470

[9] Adamovich I V, Choi I, Jiang N, Kim J H, Keshav S, Lempert W R, Mintusov E I, Nishihara M, Samimy M and Uddi M 2009 Plasma Assisted Ignition and High-Speed Flow Control: Non-Thermal and Thermal Effects *Plasma Sources Sci. Technol.* **18** 034018

[10] Starikovskaia S M and Starikovskii A Yu 2010 Plasma Assisted Ignition and Combustion *Handbook of Combustion* ed Lackner M, Winter F and Agarwal A K (Wiley-VCH) pp 71–93 ISBN 978-3-527-32449-1

[11] Vincent-Randonnier A 2010 Combustion Enhancement and Stabilization: Principles of Plasma Assistance and Diagnostic Tools *Handbook of Combustion* ed Lackner M, Winter F and Agarwal A K (Wiley-VCH) pp 125–160 ISBN 978-3-527-32449-1

[12] Starikovskiy A and Aleksandrov N 2011 Plasma–Assisted Ignition and Combustion *Aeronautics and Astronautics* ed Mulder M ISBN 978-953-307-473-3

[13] Starikovskiy A Yu and Aleksandrov N 2013 Plasma-Assisted Ignition and Combustion *Progress in Energy and Combustion Science* **39** 61–110

[14] Starikovskaia S M 2014 Plasma-Assisted Ignition and Combustion: Nanosecond Discharges and Development of Kinetic Mechanisms (Topical Review) *J. Phys. D: Appl. Phys.* **47** 353001 (34pp)

[15] Starikovskiy A 2015 Physics and Chemistry of Plasma-Assisted Combustion *Philosophical Transactions of the Royal Society A* **373** 20150074

[16] Ju Y and Sun W 2015 Plasma Assisted Combustion: Dynamics and Chemistry *Progress in Energy and Combustion Science* **48** 21–83

[17] Leonov S, Adamovich I and Soloviev V R 2016 Dynamics of Near-Surface Electric Discharges and Mechanisms of Their Interaction with the Airflow (Topical Review) *Plasma Sources Sci. Technol.* **25** 063001

[18] Alrashidi A M R N, Adam N M, Hairuddin A A and Abdullah L C 2018 A Review on Plasma Combustion of Fuel in Internal Combustion Engines *Int. J. Energy Res.* **42** 1813–1833

[19] Starikovskaia S M, Lacoste D A and Colonna G 2021 Non-Equilibrium Plasma for Ignition and Combustion Enhancement *Eur. Phys. J. D* **75**

[20] Laux C O 2022 Applications of Plasma Discharges to Combustion *Journal of the Combustion Society of Japan* **64** 257–264

[21] Popov N A and Starikovskaia S M 2022 Relaxation of Electronic Excitation in Nitrogen-Oxygen and Fuel-Air Mixtures: Fast Gas Heating in Plasma-Assisted Ignition and Flame Stabilization *Progress in Energy and Combustion Science* **91** 100928

[22] Ju Y, Mao X, Lefkowitz J K and Zhong H 2023 Plasma-Assisted Hydrogen Combustion *Hydrogen for Future Thermal Engines* Green Energy and Technology ed Tingas E A (Springer Nature Switzerland AG)

[23] Lacoste D A 2023 Flames with Plasmas *Proc. Combust. Inst.* **39** 5405–5428

[24] Ju Y and Starikovskiy A Yu 2025 *Plasma Assisted Combustion and Chemical Processing* first edition ed (Boca Raton FL: CRC Press) ISBN 978-1-032-06610-3 978-1-032-06611-0

[25] Laux C O, Perrin-Terrin J B, Lafaurie V and Starikovskaia S M 2025 Foundations of Plasma-Assisted Combustion. Part 2. Mechanisms and Applications *Plasma Sources Sci. Technol.*

[26] Guerlac H 2019 *Lavoisier - the Crucial Year. The Background and Origin of His First Experiments on Combustion in 1772.* (Cornell University Press, Ithaca, New York)

[27] Eckardt D and Rufli P 2002 Advanced Gas Turbine Technology: ABB/BCC Historical Firsts *J. Eng. Gas Turbines Power* **124(3)** 542–549

[28] Semenoff N 1927 Die Oxydation Des Phosphordampfes Bei Niedrigen Druckens *Zeitschrift für Physik* **46** 109–131

[29] Semenov N N 1934 *Chain Reactions (in Russian)* (Goskhimtechizdat, Leningrad)

[30] Thompson H W and Hinshelwood C N 1929 The Mechanism of the Homogeneous Combination of Hydrogen and Oxygen *Proc. R. Soc. London, Ser. A* **122 (790)** 610–621

[31] Thompson H W 1973 Cyril Norman Hinshelwood, 1897-1967 *Biogr. Mems Fell. R. Soc.* **19** 375–471

[32] The Nobel Prize in Chemistry 1956 https://www.nobelprize.org/prizes/chemistry/1956/summary

[33] Azatyan V V 2021 Role of Semenov's Theory of Chain Reactions in the Formation of Modern Concepts on the Processes of Combustion, Explosion and Detonation of Gases *Russian Journal of Physical Chemistry B* **15(2)** 278–284

[34] Poinsot T and Veynante D 2005 *Theoretical and Numerical Combustion* (R.T. Edwards, Inc.) ISBN 978-1-930217-10-2

[35] Warnatz J, Maas U and Dibble R W 2006 *Combustion: Physical and Chemical Fundamentals, Modeling and Simulation, Experiments, Pollutant Formation* 4th ed (Springer-Verlag Berlin Heidelberg)

[36] Liberman M 2008 *Introduction to Physics and Chemistry of Combustion: Explosion, Flame, Detonation* (Springer-Verlag Berlin Heidelberg)

[37] Zel'dovich Y B, Barenblatt G I, Librovich V B and Makhviladze G M 2011 *The Mathematical Theory of Combustion and Explosion* (Springer-Verlag New York Inc.)

[38] Law C K 2006 *Combustion Physics* (Cambridge University Press)

[39] Treurniet T C, Nieuwstadt F T M and Boersma B J 2006 Direct Numerical Simulation of Homogeneous Turbulence in Combination with Premixed Combustion at Low Mach Number Modelled by the G-equation *Journal of Fluid Mechanics* **565** 25–62

[40] Williams F A 1985 *Combustion Theory* (Boca Raton: CRC Press)

[41] Glassman I, Yetter R A and Glumac N G 2014 *Combustion* 5th ed (Academic press)

[42] Hayakawa A, Goto T, Mimoto R, Arakawa Y, Kudo T and Kobayashi H 2015 Laminar Burning Velocity and Markstein Length of Ammonia/Air Premixed Flames at Various Pressures *Fuel* **159** 98–106

[43] Borghi R 1985 On the Structure and Morphology of Turbulent Premixed Flames *Recent Advances in the Aerospace Sciences* (Springer, Boston, MA) pp 117–138 ISBN 978-1-4684-4298-4

[44] Peters N 1988 Laminar Flamelet Concepts in Turbulent Combustion *Symposium (International) on Combustion* **21** 1231–1250

[45] Lee J H S 2008 *The Detonation Phenomenon* (Cambridge University Press)

[46] Monnier V, Vidal P, Rodriguez V and Zitoun R 2023 From Graph Theory and Geometric Probabilities to a Representative Width for Three-Dimensional Detonation Cells *Combust. Flame* **256** 112996

[47] Hayes W D and Probstein R F 1959 *Hypersonic Flow Theory* (Academic press)

[48] Anderson J D 2024 *Fundamentals of Aerodynamics* seventh ed ISBN 1-264-15192-6

[49] Anderson J D 2019 *Hypersonic and High-Temperature Gas Dynamics* 3rd ed ISBN 978-1-62410-514-2

[50] Zhang F 2012 *Shock Waves Science and Technology Library, Vol. 6: Detonation Dynamics* vol 6 (Springer Science & Business Media)

[51] Semenov N N 1958 *Some Problems of Chemical Kinetics and Reactivity* (Pergamon Press)

[52] Alberty R A and Silbey R J 1992 *Physical Chemistry* (New York Chichester Brisbane [etc.]: J. Wiley & sons) ISBN 978-0-471-62181-2

[53] Emmanuel N M and Knorre D G 1974 *Lectures on Chemical Kinetics* (Vusshaia Shkola, Moscow)

[54] Gardiner Jr W C (ed) 2000 *Gas-Phase Combustion Chemistry* (Springer-Verlag New York, Inc.)

[55] Liang W and Law C K 2018 An Analysis of the Explosion Limits of Hydrogen/Oxygen Mixtures with Nonlinear Chain Reactions *Phys. Chem. Chem. Phys.* **20** 742–751

[56] Liang W and Law C K 2019 On Radical-Induced Ignition in Combustion Systems *Annual Review of Chemical and Biomolecular Engineering* **10** 199–217

[57] Wang X and Law C K 2013 An Analysis of the Explosion Limits of Hydrogen-Oxygen Mixtures *The Journal of Chemical Physics* **138** 134305

[58] Boivin P, Le Boursicaud M, Millán-Merino A, Taileb S, Melguizo-Gavilanes J and Williams F 2023 Hydrogen Ignition and Safety *Hydrogen for Future Thermal Engines* Green Energy and Technology (Springer) pp 161–236 ISBN 978-3-031-28411-3

[59] Wang Z, Gou X and Zhang H 2024 Explosion Limit of Hydrogen/Oxygen Mixture with Water Vapor Addition *International Journal of Hydrogen Energy* **50** 772–781

[60] Semenov N N 1958 *Concerning Some Problems of Chemical Kinetics and Chemical Reactivity (Free Radicals and Chain Reactions)* (Moscow: USSR Academy of Science Publ.)

[61] Petersen E L, Röhrig M, Davidson D F, Hanson R K and Bowman C T 1996 High-Pressure Methane Oxidation behind Reflected Shock Waves *Twenty-Sixth International Symposium on Combustion* vol 26 (The Combustion Institute) pp 799–806

[62] Frenklach M, Wang H, Goldenberg M, Smith G P, Golden D M, Bowman C T, Hanson R K, Gardiner W C and Lissianski V 1995 Report No. GRI-95/0058 Tech. rep. Gas Research Institute

[63] Smith G P, Golden D M, Frenklach M, Moriarty N W, Eiteneer B, Goldenberg M, Bowman C T, Hanson R K, Song S, Gardiner W C Jr, Lissianski V V and Qin Z 1999 GRI-mech 3.0

[64] Petersen E L, Davidson D F and Hanson R K 1999 Kinetics Modeling of Shock-Induced Ignition in Low-Dilution CH_4/O_2 Mixtures at High Pressures and Intermediate Temperatures *Combust. Flame* **117** 272–290

[65] Healy D, Curran H J, Simmie J M, Kalitan D M, Zinner C M, Barrett A B, Petersen E L and Bourque G 2008 Methane/Ethane/Propane Mixture Oxidation at High Pressures and at High, Intermediate, and Low Temperatures *Combust. Flame* **155** 441–448

[66] Healy D, Kalitan D M, Aul C J, Petersen E L, Bourque G and Curran H J 2010 Oxidation of C_1—C_5 Alkane Quinternary Natural Gas Mixtures at High Pressures *Energy Fuels* **24** 1521–1528

[67] Heufer K A, Bugler J and Curran H J 2013 A Comparison of Longer Alkane and Alcohol Ignition Including New Experimental Results for n–Pentanol and n–Hexanol *Proc. Combust. Inst.* **34** 511–518

[68] Combustion Chemistry Centre, Online Combustion Mechanisms https://universityofgalway.ie/combustionchemistrycentre/mechanismdownloads/

[69] Zhang P, Zsély I G, Samu V, Nagy T and Turányi T 2021 Comparison of Methane Combustion Mechanisms Using Shock Tube and Rapid Compression Machine Ignition Delay Time Measurements *Energy & Fuels* **35** 12329–12351

[70] Zhang P, Zsély I G, Papp M, Nagy T and Turányi T 2022 Comparison of Methane Combustion Mechanisms Using Laminar Burning Velocity Measurements *Combust. Flame* **238** 111867

[71] NUI Galway Combustion Chemistry Centre 2017 AramcoMech 2.0

[72] The FORCE - California Institute of Technology 2015 CaltechMech Detailed Kinetic Model (Version 2.3)

[73] Glarborg P, Miller J A, Ruscic B and Klippenstein S J 2018 Modeling Nitrogen Chemistry in Combustion *Progress in Energy and Combustion Science* **67** 31–68

[74] Mechanical and Aerospace Engineering (Combustion Research) University of California at San Diego 2014 Chemical-Kinetic Mechanisms for Combustion Applications. San Diego Mechanism

[75] Smith G P, Tao Y and Wang H 2016 Foundational Fuel Chemistry Model Version 1.0

[76] Wu Y, Panigrahy S, Sahu A B, Bariki C, Beeckmann J, Liang J, Mo-hamed A A E, Dong S, Tang C, Pitsch H, Huang Z and Curran H J 2021 Understanding the Antagonistic Effect of Methanol as a Component in Surrogate Fuel Models: A Case Study of Methanol/n-Heptane Mixtures *Combust. Flame* **226** 229–242

[77] Konnov A A 2009 Implementation of the NCN Pathway of Prompt-NO Formation in the Detailed Reaction Mechanism *Combust. Flame* **156** 2093–2105

[78] Choudhary R, Biswas P, Boddapati V, Wang H and Hanson R K 2025 LT-HyChem-A Physics-Based Chemical Kinetic Modeling Approach for Low-Temperature Oxidation of Real Fuels I: Rationale, Methodology, and Application to a Simple Fuel Mixture *Combustion and Flame* **271** 113852

[79] Ju Y 2021 Understanding Cool Flames and Warm Flames *Proceedings of the Combustion Institute* **38** 83–119

[80] Filimonova EA 2014 Discharge Effect on the Negative Temperature Coefficient Behaviour and Multistage Ignition in C3H8-air Mixture *Journal of Physics D: Applied Physics* **48** 015201

[81] Sorrentino G, Ariemma G B, Ferraro F and Fiorina B 2024 Including Detailed Chemistry Features in the Modeling of Emerging Low-Temperature Reactive Flows: A Review on the Application to Diluted and MILD Combustion Systems *Applications in Energy and Combustion Science* **20** 100291

[82] Peters N 2001 Turbulent Combustion *Measurement Science and Technology* **12** 2022

[83] Jangi M and Bai X S 2012 Multidimensional Chemistry Coordinate Mapping Approach for Combustion Modelling with Finite-Rate Chemistry *Combustion Theory and Modelling* **16** 1109–1132

[84] Hodzic E, Jangi M, Szasz R Z and Bai X S 2017 Large Eddy Simulation of Bluff Body Flames Close to Blow-off Using an Eulerian Stochastic Field Method *Combustion and Flame* **181** 1–15

[85] Raizer Yu P 2011 *Gas Discharge Physics* (Springer Berlin Heidelberg) ISBN 978-3-642-64760-4

[86] Fortov V E, Iakubov I T and Khrapak A G 2006 *Physics of Strongly Coupled Plasma* (Clarendon Press)

[87] Artsimovich A A and Sagdeev R Z 1979 *Plasma physics for physicists* (Atomizdat)

[88] Smirnov B M 2001 *Physics of Ionized Gases* (New York, Chichester, Weinheim, Brisbane, Singapore, Toronto: John Wiley and Sons, Inc.)

[89] Fridman A 2008 *Plasma Chemistry* (Cambridge University Press) ISBN 978-0-521-84735-3

[90] Lieberman M A and Lichtenberg A J 2005 *Principles of Plasma Discharges and Materials Processing* 2nd ed (John Wiley & Sons) ISBN 0-471-72001-1

[91] Chabert P and Braithwaite N 2011 *Physics of Radio-Frequency Plasmas* (Cambridge University Press)

[92] Ebeling W, Kraeft W D and Kremp D 1976 *Theory of Bound States and Ionization Equilibrium in Plasmas and Solids* (Akademie-Verlag)

[93] Bruggeman P J, Bogaerts A, Pouvesle J M, Robert E and Szili E J 2021 Plasma–Liquid Interactions *Journal of Applied Physics* **130** 200401

[94] Radzig A A and Smirnov B M 2012 *Reference Data on Atoms, Molecules, and Ions* vol 31 (Springer Science & Business Media)

[95] Eriksson K B and Isberg H B S 1968 New Measurements in Spectrum of Atomic Oxygen OI *Arkiv for Fysik* **37** 221

[96] Qi F, Sheng L, Zhang Y, Yu S and Li W 1995 Experimental and Theoretical Study of the Dissociation Energies D0 (H2N H) and D0 (H2N\protext{$^+$} H) and Other Related Quantities *Chemical physics letters* **234** 450–454

[97] Eriksson K B S and Pettersson J E 1971 New Measurements in the Spectrum of the Neutral Nitrogen Atom *Physica Scripta* **3** 211

[98] Kandula D Z, Gohle C, Pinkert T J, Ubachs W and Eikema K S 2010 Extreme Ultraviolet Frequency Comb Metrology *Physical Review Letters* **105** 063001

[99] Petrovic Z Lj, Dujko S, Maric D, Malovic G, Nikitovic Z, Sasic O, Jovanovic J, Stojanovic V and Radmilovic-Radenovic M 2009 Measurement and Interpretation of Swarm Parameters and Their Application in Plasma Modelling *J. Phys. D: Appl. Phys.* **42** 194002

[100] Korolov I, Vass M and Donkó Z 2016 Scanning Drift Tube Measurements of Electron Transport Parameters in Different Gases: Argon, Synthetic Air, Methane and Deuterium *J. Phys. D: Appl. Phys.* **49** 415203

[101] Petrovic Z Lj, Suvakov M, Nikitovic Z, Dujko S, Sasic O, Jovanovic J, Malovic G and Stojanovic V 2007 Kinetic Phenomena in Charged Particle Transport in Gases, Swarm Parameters and Cross Section Data (Topical Review) *Plasma Sources Sci. Technol.* **16** S1–S12

[102] Huxley L G H and Crompton R W 1974 *The Diffusion and Drift of Electrons in Gases* john wiley & sons ed (New-York: John Wiley and Sons)

[103] Korolov I, Vass M, Bastykova N Kh and Donkó Z 2016 A Scanning Drift Tube Apparatus for Spatiotemporal Mapping of Electron Swarms *Rev. Sci. Instr.* **87**

[104] Mesyats G A 2006 Similarity Laws for Pulsed Gas Discharges *Physics-Uspekhi* **49** 1045

[105] Korolev Y D and Mesyats GA 2001 Physics of Pulsed Breakdown in Gases *IEEE Electrical Insulation Magazine* **17** 60–61

[106] Al-Amin SAJ, Kucukarpaci HN and Lucas J 1985 Electron Swarm Parameters in Oxygen and Methane *Journal of Physics D: Applied Physics* **18** 1781

[107] Schmidt B and Roncossek M 1992 Drift Velocity, Longitudinal and Transverse Diffusion in Hydrocarbons Derived from Distributions of Single Electrons *Australian journal of physics* **45** 351–364

[108] Davies DK, Kline LE and Bies WE 1989 Measurements of Swarm Parameters and Derived Electron Collision Cross Sections in Methane *Journal of Applied physics* **65** 3311–3323

[109] Hunter SR, Carter JG and Christophorou LG 1986 Electron Transport Measurements in Methane Using an Improved Pulsed Townsend Technique *Journal of applied physics* **60** 24–35

[110] Berghöfer T, Blümer J and Hörandel JR 2004 A Measurement of Drift Velocities of Electrons in Xenon–Methane Mixtures *Nuclear Instruments and Methods in Physics Research Section A: Accelerators, Spectrometers, Detectors and Associated Equipment* **525** 544–552

[111] Yoshida K, Ohshima T, Ohmori Y, Ohuchi H and Tagashira H 1996 The Measurement of Electron Transport Coefficients in Methane by a Double-Shutter Drift Tube Method Combined with ATS Analysis *Journal of Physics D: Applied Physics* **29** 1209

[112] Aleksandrov N L and Son E E 1980 Energy distribution and swarm parameters of electrons in gases under the action of electric field *Plasma chemistry* vol 7 ed Smirnov B M (Moscow: Atomizdat Publ.) pp 35–75

[113] Slovetsky D I 1980 *Mechanisms of chemical reactions in nonequilibrium plasma* (Moscow: Nauka Publishing)

[114] Hagelaar G J M and Pitchford L C 2005 Solving the Boltzmann Equation to Obtain Electron Transport Coefficients and Rate Coefficients for Fluid Models *Plasma Sources Sci. Technol.* **14** 722

[115] Kortshagen U, Busch C and Tsendin L D 1996 On Simplifying Approaches to the Solution of the Boltzmann Equation in Spatially Inhomogeneous Plasmas *Plasma Sources Sci. Technol.* **5** 1

[116] Mitchner M and Kruger C H 1973 *Partially Ionized Gases* Wiley Series in Plasma Physics (New York: John Wiley and Sons, Inc.) ISBN 978-0-471-61172-1

[117] Laux C O 2002 Radiation and Nonequilibrium Collisional-Radiative Models *VKI Special Course on Physico-Chemical Models for High Enthalpy and Plasma Flows Modeling* pp 125–138

[118] Demtröder W 2006 *Atoms, Molecules, and Photons: An Introduction to Atomic-, Molecular-, and Quantum-Physics* (Berlin ; New York: Springer) ISBN 978-3-540-20631-6

[119] Ochkin V N 2009 *Spectroscopy of Low Temperature Plasma* (Weinheim: Wiley-VCH) ISBN 978-3-527-40778-1

[120] Paris P, Aints M, Valk F, Plank T, Haljaste A, Kozlov K V and Wagner H E 2005 J. Phys. D: Appl. Phys. **38** 3894

[121] Obrusnik A, Bilek P, Hoder T, Simek M and Bonaventura Z 2018 Plasma Sources Sci. Technol. **27** 085013

[122] Lepikhin N D, Popov N A and Starikovskaia S M 2022 On Electric Field Measurements Based on Intensity Ratio of 1^- and 2^+ Systems of Nitrogen in Discharges with High Specific Deposited Energy *Plasma Sources Sci. Technol.* **31** 084002

[123] AliCherif M, Masuda R, Claverie A, Starikovskaia S and Vidal P 2024 Plasma-Enhanced Detonability: Experimental and Calculated Reduction of the Detonation Cell Size *Combust. Flame* **268** 113639

[124] Starik A M and Titova N S 2001 Initiation of Combustion and Detonation in Gas Mixtures under Excitation of the Molecule Oxygen in $O_2(a^1\Delta_g)$ State *Chemical Physics Reports* **20** 17

[125] Popov N A 2001 Investigation of the Mechanism for Rapid Heating of Nitrogen and Air in Gas Discharges *Plasma Phys. Rep.* **27** 886–896

[126] Popov N A 2011 Effect of Singlet Oxygen $O_2(a^1\Delta_g)$ Molecules Produced in a Gas Discharge Plasma on the Ignition of Hydrogen–Oxygen Mixtures *Plasma Sources Sci. Technol.* **20** 045002

[127] Kosarev I N, Aleksandrov N L, Kindysheva S V, Starikovskaia S M and Starikovskii A Yu 2008 Kinetics of Ignition of Saturated Hydrocarbons by Nonequilibrium Plasma: CH_4–Containing Mixtures *Combust. Flame* **154** 221–233

[128] Kosarev I N, Aleksandrov N L, Kindysheva S V, Starikovskaia S M and Starikovskii A Yu 2009 Kinetics of Ignition of Saturated Hydrocarbons by Nonequilibrium Plasma: C_2H_6– to C_5H_{12}–Containing Mixtures *Combust. Flame* **156** 221–233

[129] Bogaerts A, Wang W, Berthelot A and Guerra V 2016 Modeling Plasma-Based CO_2 Conversion: Crucial Role of the Dissociation Cross Section

[130] Morillo-Candas A S, Silva T, Klarenaar B L M, Grofulović M, Guerra V and Guaitella O 2020 Electron Impact Dissociation of CO_2 *Plasma Sources Sci. Technol.* **29** 01LT01

[131] Scherer N F, Knee J L, Smith D D and Zewail A H 1985 Femtosecond Photofragment Spectroscopy: The Reaction ICN → CN + I *The Journal of Physical Chemistry* **89** 5141–5143

[132] Rusterholtz D L, Lacoste D A, Stancu G D, Pai D Z and Laux C O 2013 Ultrafast Heating and Oxygen Dissociation in Atmospheric Pressure Air by Nanosecond Repetitively Pulsed Discharges *J. Phys. D: Appl. Phys.* **46** 464010

[133] Lepikhin N D, Popov N A and Starikovskaia S M 2018 Fast Gas Heating and Radial Distribution of Active Species in Nanosecond Capillary Discharge in Pure Nitrogen and N_2:O_2 Mixtures *Plasma Sources Sci. Technol.* **27** 055005

[134] Shu Z, Popov N A and Starikovskaia S M 2024 Absolute Calibration of the Ratio of Xe/O_2 Two-Photon Absorption Cross-Sections for O-TALIF Applications *Plasma Sources Sci. Technol.* **33** 025019

[135] Popov N A 2016 Kinetics of Plasma-Assisted Combustion: Effect of Non-Equilibrium Excitation on the Ignition and Oxidation of Combustible Mixtures *Plasma Sources Sci. Technol.* **25** 043002

[136] Polak L S and Slovetsky D I 1976 Electron Impact Induced Electronic Excitation and Molecular Dissociation *International Journal for Radiation Physics and Chemistry* **8** 257–282

[137] Slovetsky D I 1974 Dissociation of Molecules by Electron Impact (Review) *Plasma Chemistry* **1** 156–202

[138] Reiter D, Baelmans M and Boerner P 2005 The EIRENE and B2-EIRENE Codes *Fusion science and technology* **47** 172–186

[139] WebEIRENE https://www.eirene.de/index.html

[140] Janev RK and Reiter D 2003 Unified Analytic Representation of Hydrocarbon Impurity Collision Cross-Sections *Journal of nuclear materials* **313** 1202–1205

[141] Okabe H *et al.* 1978 *Photochemistry of Small Molecules* vol 431 (Wiley New York)

[142] Corrigan S J B 1965 Dissociation of Molecular Hydrogen by Electron Impact *J. Chem Phys* **43** 4381

[143] Manton J E and Tickner A W 1960 The Decomposition of Methane by Low-Energy Electrons *Can. J. Chem.* **38** 858–868

[144] Slovetsky D I 1988 Mechanisms of Decomposition of Hydrocarbons in Electrical Discharges *Pure and Applied Chemistry* **60** 753–768

[145] Orel I 2020 *Measurements of Electric Field and Dissociated Species in Nanosecond Discharges for Kinetic and Biological Applications* Ph.D. thesis Institut Polytechnique de Paris

[146] Popov N A 2016 Pulsed Nanosecond Discharge in Air at High Specific Deposited Energy: Fast Gas Heating and Active Particle Production *Plasma Sources Sci. Technol.* **25** 044003

[147] Klimov A I, Mishin G I, Fedotov A B and Shakhovatov V A 1989 Propagation of shock waves in DC discharge *Tech. Phys. Lett.* **15** 31–36

[148] Ono R, Teramoto Y and Oda T 2010 Gas Density in a Pulsed Positive Streamer Measured Using Laser Shadowgraph *Journal of Physics D: Applied Physics* **43** 345203

[149] Xu D, Shneider M N, Lacoste D A and Laux C O 2014 Thermal and Hydrodynamic Effects of Nanosecond Discharges in Atmospheric Pressure Air *Journal of Physics D: Applied Physics* **47** 235202

[150] Mintoussov E I, Pendleton S J, Gerbault F G, Popov NA and Starikovskaia SM 2011 Fast Gas Heating in Nitrogen–Oxygen Discharge Plasma: II. Energy Exchange in the Afterglow of a Volume Nanosecond Discharge at Moderate Pressures *Journal of Physics D: Applied Physics* **44** 285202

[151] Aleksandrov N L, Kindysheva S V, Nudnova M M and Starikovskiy A 2010 Mechanism of Ultra-Fast Heating in a Non-Equilibrium Weakly Ionized Air Discharge Plasma in High Electric Fields *Journal of Physics D: Applied Physics* **43** 255201

[152] Bruggeman P J, Sadeghi N, Schram D C and Linss V 2014 Gas Temperature Determination from Rotational Lines in Non-Equilibrium Plasmas: A Review *Plasma Sources Sci. Technol.* **23** 023001

[153] Tibère-Inglesse A, McGuire S and Laux C 2023 Inferring Gas Temperature from N_2 Emission via Rotational Distribution of the N_2 $B^3\Pi_g$ and $C^3\Pi_u$ States *Plasma Sources Sci. Technol.* **32** 075018

[154] Popov N A 2011 Fast Gas Heating in a Nitrogen–Oxygen Discharge Plasma: I. Kinetic Mechanism *Journal of Physics D: Applied Physics* **44** 285201

[155] Capitelli M, Ferreira C M, Gordiets B F and Osipov A I 2012 *Plasma Kinetics in Atmospherics Gases* (Springer–Verlag) ISBN 987-3-642-08683-0

[156] Capitelli M, Colonna G and D'Angola A 2012 *Fundamental Aspects of Plasma Chemical Physics* (Springer–Verlag) ISBN 987-1-4419-8181-3

[157] Nijdam S, Teunissen J and Ebert U 2020 The Physics of Streamer Discharge Phenomena *Plasma Sources Science and Technology* **29** 103001

[158] Kobayashi S, Bonaventura Z, Tholin F, Popov N A and Bourdon A 2017 Study of Nanosecond Discharges in H2–Air Mixtures at Atmospheric Pressure for Plasma Assisted Combustion Applications *Plasma Sources Science and Technology* **26** 075004

[159] Doyle S J, Dias T C, Meyer M and Kushner M J 2025 Controlling Plasma Produced Fluxes to Liquid Surfaces by Acoustic Structuring: Applications to Plasma Driven Solution Electrochemistry *Plasma Sources Science and Technology* **34** 035004

[160] Babaeva N Y, Tereshonok D V and Naidis G V 2016 Fluid and Hybrid Modeling of Nanosecond Surface Discharges: Effect of Polarity and Secondary Electrons Emission *Plasma Sources Science and Technology* **25** 044008

[161] Yin B, Zhu Y, Wang X and Wu Y 2025 Dynamics Characterization of Spiral-Tubular Dielectric Barrier Discharge Based on Experiment and Simulation *Physics of Plasmas* **32** 093503

[162] PASSKEy, Howpublished = http://www.plasma-tech.net/parser/passkey/

[163] Phelps A V, Jelenković B M and Pitchford L C 1987 Simplified Models of Electron Excitation and Ionization at Very High E/n *Physical Review A* **36** 5327–5336

[164] Dorai R, Hassouni K and Kushner M J 2000 Interaction between Soot Particles and NO x during Dielectric Barrier Discharge Plasma Remediation of Simulated Diesel Exhaust *Journal of applied physics* **88** 6060–6071

[165] Stafford D S and Kushner M J 2004 O2 (Δ1) Production in He/ O2 Mixtures in Flowing Low Pressure Plasmas *Journal of applied physics* **96** 2451–2465

[166] MIPSE https:mipse.umich.edu/index.php

[167] BOLSIG+ https://www.bolsig.laplace.univ-tlse.fr

[168] Phelps A V and Pitchford L C 1985 Anisotropic Scattering of Electrons by N_2 and Its Effect on Electron Transport *Phys. Rev. A* **31** 2932–2949

[169] Itikawa Yu 2006 Cross Sections for Electron Collisions with Nitrogen Molecules *J. Phys. Chem. Ref. Data* **35** 31–53

[170] Su H, Cheng X, Zhang H and Tennyson J 2021 Electron Collisions with Molecular Nitrogen in Its Ground and Electronically Excited States Using the R-matrix Method *J. Phys. B: At. Mol. Opt. Phys.* **54** 12

[171] Blasko J, Orszagh J, Stachova B and Matejcık S 2023 Spectral Electron Energy Map of Electron Impact Induced Emission of Nitrogen *Eur. Phys. J. D* **77** 11

[172] Pitchford L C 2013 GEC Plasma Data Exchange Project (Preface) *J. Phys. D: Appl. Phys.* **46** 2

[173] Pancheshnyi S, Biagi S, Bordage M C, Hagelaar G J M, Morgan W L, Phelps A V and Pitchford L C 2012 The LXCat Project: Electron Scattering Cross Sections and Swarm Parameters for Low Temperature Plasma Modeling *Chemical Physics* **398** 148–153

[174] LXCat https://nl.lxcat.net/home/

[175] Pancheshnyi S, Eismann B, Hagelaar G J M and Pitchford L C 2008 ZDPlasKin Tech. rep. University of Toulouse, LAPLACE, CNRS-UPS-INP

[176] Markosyan A H, Luque A, Gordillo-Vázquez F J and Ebert U 2014 PumpKin: A Tool to Find Principal Pathways in Plasma Chemical Models *Comput. Phys. Commun.* **185** 2697

[177] LoKI https://nprime.tecnico.ulisboa.pt/loki, https://github.com/IST-Lisbon/LoKI

[178] Tejero-del-Caz A, Guerra V, Gonçalves D, Lino da Silva M, Marques L, Pinhão N, Pintassilgo C D and Alves L L 2019 The LisbOn Kinetics Boltzmann Solver *Plasma Sources Sci. Technol.* **28** 21

[179] Tejero-del-Caz A, Guerra V, Pinhão N, Pintassilgo C D and Alves L L 2021 On the Quasi-Stationary Approach to Solve the Electron Boltzmann Equation in Pulsed Plasmas *Plasma Sources Sci. Technol.* **30** 15

[180] BOLOS Solver https://github.com/aluque/bolos/blob/master/README.rst

[181] Aleksandrov N L, Dyatko N A and Kochetov I V 1995 Rate of Inelastic Electron Processes in a Weakly Ionized Plasma in a Nonstationary Electric Field *Plasma Phys. Rep.* **21** 763–767

[182] Kochetov I V and Aleksandrov N L 2018 The Effect of Fuel Oxidation on Electron Swarm Properties and Nanosecond Discharge Characteristics in Combustible Mixtures *Plasma Sources Sci. Technol.* **27** 115004

[183] Anokhin E M, Popov M A, Kochetov I V, Aleksandrov N L and Starikovskii A Yu 2016 Plasma Decay in High-Voltage Nanosecond Discharges in Oxygen-Containing Mixture *Plasma Physics Reports* **42** 59–67

[184] Dias T C and Guerra V 2023 Assessment of Time-Locality Assumptions on the Modeling of Nanosecond-Pulsed Discharges *XXXV International Conference on Phenomena in Ionized Gases (ICPIG)* (Egmond aan Zee, the Netherlands)

[185] Dias T C and Guerra V 2025 Are Local-Field and Local-Energy Approximations Appropriate for Modelling Nanosecond Discharges? *J. Phys. D: Appl. Phys.* **58** 185204

[186] Alves L L, Becker M M, van Dijk J, Gans T, Go D B, Stapelmann K, Tennyson J, Turner M M and Kushner M J 2023 Foundations of Plasma Standards (Topical Review) *Plasma Sources Sci. Technol.* **32** 32

[187] Adamovich I V, Li T and Lempert W R 2015 Kinetic Mechanism of Molecular Energy Transfer and Chemical Reactions in Low-Temperature Air-Fuel Plasmas *Philosophical Transactions of the Royal Society A: Mathematical, Physical and Engineering Sciences* **373** 20140336

[188] ANSYS https://www.ansys.com/fr-fr/products/fluids/ansys-chemkin

[189] Goodwin D G, Moffat H K and Speth R L 2017 Cantera: An Object-Oriented Software Toolkit for Chemical Kinetics, Thermodynamics, and Transport Processes. Version 2.3. 0 *Zenodo*

[190] Sallam K and Srivastava S 2023 *An Introduction to Combustion with Applications Using Cantera* (Cambridge Scholars Publishing)

[191] Shahsavari M, Konnov A A, Valera-Medina A and Jangi M 2022 On Nanosecond Plasma-Assisted Ammonia Combustion: Effects of Pulse and Mixture Properties *Combust. Flame* **245** 112368

[192] Dijoud R J, Laws N and Guerra-Garcia C 2025 Mapping the Performance Envelope and Energy Pathways of Plasma-Assisted Ignition across Combustion Environments *Combustion and Flame* **271** 113793

[193] Qiu Y, Zhu Y, Wu Y, Zhao N, Li Z, Hao M, Zhang B and Pan D 2023 Numerical Investigation of the Hybrid Pulse–DC Plasma Assisted Ignition and NOx Emission of NH3/N2/O2 Mixture *Combustion and Flame* **258** 113078

[194] Lutz A E, Kee R J and Miller J A 1988 SENKIN: A FORTRAN Program for Predicting Homogeneous Gas Phase Chemical Kinetics with Sensitivity Analysis Technical Report Sandia National Laboratories Livermore, CA (USA)

[195] Shao X, Lacoste D A and Im H G 2024 ChemPlasKin: A General-Purpose Program for Unified Gas and Plasma Kinetics Simulations *Applications in Energy and Combustion Science* **19** 100280

[196] Atkinson R, Baulch D L, Cox R A, Crowley J N, Hampson R F, Hynes R G, Jenkin M E, Rossi M J and Troe J 2004 Evaluated Kinetic and Photochemical Data for Atmospheric Chemistry: Volume I - Gas Phase Reactions of Ox, HOx, NOx and SOx Species *Atmos. Chem. Phys.* **4** 1461–1738

[197] IUPAC Publications https://list.iupac.org/publications/

[198] Kossyi I A, Kostinsky A Y, Matveyev A A and Silakov V P 1992 Kinetic Scheme of the Non-Equilibrium Discharge in Nitrogen-Oxygen Mixtures *Plasma Sources Sci. Technol.* **1** 207